STRUCTURE, SURFACES, AND COMPOSITION OF CATALYTIC NANOPARTICLES FROM QUANTITATIVE ABERRATION CORRECTED TRANSMISSION ELECTRON MICROSCOPY

STRUCTURE, SURFACES, AND COMPOSITION OF CATALYTIC NANOPARTICLES FROM QUANTITATIVE ABERRATION CORRECTED TRANSMISSION ELECTRON MICROSCOPY

By

MICKEY CHAN, BASc.

A Thesis

Submitted to the School of Graduate Studies

In Partial Fulfillment of the Requirements

For the Degree

Master of Applied Science

McMaster University

© Copyright by Mickey Chan, June 2012

MASTER OF APPLIED SCIENCE (2012)   McMaster University

(Materials Science and Engineering)   Hamilton, Ontario

TITLE:	Structure, Surfaces, and Composition of Catalytic Nanoparticles from Quantitative Aberration Corrected Transmission Electron Microscopy
AUTHOR:	Mickey Chan, BASc. (University of Waterloo)
SUPERVISOR:	Professor Gianluigi A. Botton
NUMBER OF PAGES:	xii, 84

ABSTRACT

Proton exchange membrane fuel cells (PEMFC) are a technology of high interest for the automotive and power generation industry. The catalyst layer plays a critical role in fuel cells as it is responsible for catalyzing hydrogen oxidation and oxygen reduction to generate electricity. The current challenge in catalyst development is to produce highly active and economical catalysts. This challenge cannot be overcome without an accurate understanding of catalyst surfaces and morphology since the catalytic reactions occur on the surface active sites. Transmission electron microscopy (TEM) is an excellent tool to understand the structures of the nanoparticles down to the atomic level in determining the relationship with the catalyst's performance in fuel cell applications. Platinum (Pt) is one of the best commercially available catalysts for PEMFC due to its highly active, inert, and relatively stable properties. However, Pt is a rare precious metal due to its low abundance and high demand. Further research is aimed at developing highly active and more economical catalysts in order to mass produce PEMFC. A strategic approach is to use platinum bimetallic alloys, which greatly reduce the platinum loading as they enhance the oxygen reduction reaction [1], [2]. A detailed understanding of the nanoparticle surface is critical as the catalyst surface strongly determines its catalytic activity. Furthermore, another challenge in utilizing fuel cells is the life-time of the catalysts. It is known that electrochemical cycling affects Pt alloys. As a result, the understanding of the effect of electrochemical treatments on the catalyst's

morphology and composition is key to improving the fuel cell's performance and durability. This thesis demonstrates that through the use of TEM, useful insights regarding the morphology, surfaces, and compositions of the catalysts can be gained and contribute to the improvement in catalyst development for next generation fuel cells.

ACKNOWLEDGEMENTS

sorts of technical issues with the microscopes. I always have the feeling that nothing could go wrong with their presence.

This acknowledgement would not be complete without thanking my friends and family, especially Justine Eng, who spent her precious time proofreading my manuscript as I was writing. Thank you for all your useful comments and supports.

There were bumps and bruises during my graduate student career, but the support from all of you drove my project to completion. Your generous words of encouragement are what motivated me to work hard. Thank you.

CONTENTS

LIST OF FIGURES

LIST OF ABBREVIATIONS

ADF	Annular Dark Field
BF	Bright Field
DF	Dark Field
DFT	Density Function Theory
E-Cycling	Electrochemical Cycling
EDXS	Energy Dispersive X-ray Spectrometry
HAADF	High Angle Annular Dark Field
HOR	Hydrogen Oxidation Reaction
IL-TEM	Identical Location Transmission Electron Microscopy
NPD	Nano Probe Diffraction
ORR	Oxygen Reduction Reaction
PEMFC	Proton Exchange Membrane Fuel Cell
RHE	Reverse Hydrogen Electrode
STEM	Scanning Transmission Electron Microscopy
Ta	Annealing Temperature
Tc	Critical Temperature
TEM	Transmission Electron Microscopy
XRD	X-Ray Diffraction

1. INTRODUCTION

With the petroleum reservoir gradually being exhausted and the world population growing, there is an increasing demand for an alternative clean energy system. Extensive research has been done to develop a replacement of our conventional energy conversion devices such as batteries and heat engines. Proton exchange membrane fuel cell (PEMFC) is currently one of the most studied fields of research. It is the most promising clean energy systems with higher efficiency than the current combustion engines. With the use of hydrogen as input, not only does this element produce higher energy output, but it is also non- polluting and the most abundant chemical element. However, similar to any new technology in development, there are a number of challenges and obstacles that must be resolved in order to commercially mass produce the system. Some key challenges include high production cost as well as high catalytic activity attributed to the catalyst layer of the fuel cell compartment. As a result, one of the current research focuses is placed on catalyst development to make fuel cell production feasible as a future energy technology.

1.1. PROTON EXCHANGE MEMBRANE FUEL CELL

A proton exchange membrane fuel cell (PEMFC) is simply an electrochemical device that converts chemical energy to electrical energy. Referring to Figure 1-1 below, a fuel cell consists of two electrodes (the catalyst layer and the gas diffusion layer), and

a semi-permeable membrane. The input of hydrogen is on the anode, which is split into hydrogen atoms through which the resultant electron passes an external circuit to produce electricity. The hydrogen ions then pass through the membrane, combining with oxygen at the anode to produce water. This energy conversion process is clean and environmentally friendly as it is not producing any harmful by- products. Hydrogen fuel cells are regarded as highly efficient energy conversion system that could be developed for transport and portable fuel cell applications. As part of the component of the electrode, the catalyst layer plays a key role as it is responsible for the splitting of the hydrogen molecule. This is done by the attachment and detachment of hydrogen and oxygen on the active sites of the catalyst particles.
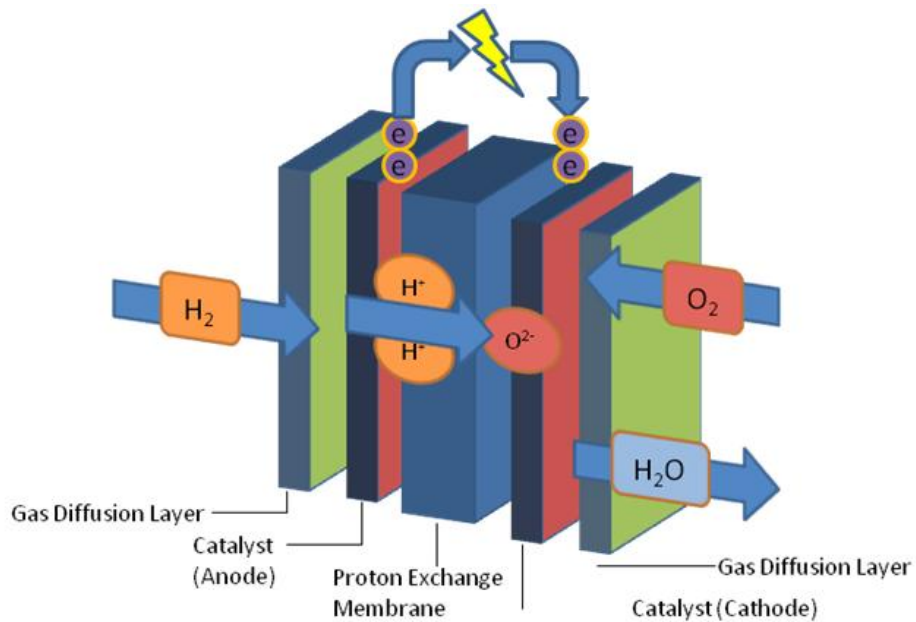
FIGURE 1-1 GENERAL SCHEMATICS OF PROTON EXCHANGE MEMBRANE FUEL CELL

Platinum is the best commercially available option for the oxygen reduction reaction due to its stable, inert, and high activity properties. However, platinum is an expensive noble metal with low abundance on Earth. [1], [2] There is currently insufficient amounts of platinum on Earth to replace all the cars in the market. Some of the major challenges in catalyst development include high cost, insufficient activity, and low stability. [2] The current research direction is to develop alternative catalysts including the use of non-noble metal, doped graphene, as well as platinum alloys. Table 1-1 below tabulates the price of various materials as acquired on June 1st, 2012 from kitco.com. As shown in the table, non-noble transition metals including iron, cobalt, copper, and nickel are much more economical compared with the other metals but they produces an inadequate oxygen reduction reaction (ORR) activity. On the other hand, platinum yields great activity but suffers from high material cost. As a result, a strategic approach is to minimize the amount of platinum usage by combining platinum with non-noble metals.

TABLE 1-1 PRICE CHART OF VARIOUS EARTH METALS

Material	Fe	Cu	Ni	Co	Ag	Ru	Ir	Pd	Pt	Au
Price per oz (USD)	0.03	0.24	1.105	1.11	28	380	450	625	1480	1626

The usage of platinum alloy not only minimizes the usage of Pt, but also enhances the catalytic activity compared with pure platinum. It has been proven that by introducing a

non- noble metal into platinum (Co, Fe, Ni, Cu) , the ORR activity increases by two to four folds compared with Pt catalyst. This is primarily due to the compression of the unit cell, which leads to a change in the surface electronic structure, hence producing high ORR activities. [3–5] Furthermore, Norskov et al. performed density functional theory simulations and showed that alloyed platinum has smaller oxygen binding energies than pure platinum [6]. In addition, most Pt alloys displayed better stability than pure platinum. All in all, research literature has proven platinum alloy to be a feasible and promising catalyst candidate with reduced platinum usage, enhanced activity, and greater stability.

As mentioned earlier, the ORR activity occurs on the active sites of the catalysts which are on the surfaces of the particles. A logical approach is to synthesize nano-sized particles to increase the surface area to volume ratio. With such approach, the effect of particle morphology and composition on electrochemistry should be considered. Ultimately, the surfaces of the catalytic nanoparticles should be studied and understood at the atomic level as the active sites are where the reactions are taking place. Transmission electron microscopy is highly effective in the study of catalytic nanoparticles as it is capable of obtaining morphological and composition information. Specifically, aberration corrected transmission electron microscopes can reveal the surface structures and atomic arrangements down to the atomic scale for a better understanding of the catalytic ability. In general, microscopy studies of catalyst

nanoparticles could help fine-tune their catalytic performance for enhanced fuel cell applications.

2. LITERATURE REVIEW

2.1. PLATINUM ALLOY AS FUEL CELL CATALYSTS

Numerous publications have demonstrated that the activity of platinum catalysts can be improved by alloying platinum with non-noble 3d metals such as Fe, Co, Ni, and Cu. It has been shown that strain is introduced into the platinum crystal when a transition metal is added to the system. This is attributed to the smaller atomic diameter compared with platinum, which results in a compressed unit cell with a decrease in Pt-Pt distance. [7] The induced strain modifies the electronic configuration, allowing a more favorable dissociative absorption of oxygen. Stamenkovic et. al. [8] used density function theory (DFT) and modeled cell potential as a function of oxygen chemisorptions energy for platinum and various bimetallic 3d platinum alloys. It should be noted that the oxygen reduction reaction (ORR) is the primary study of interest due to the fact that ORR is the rate determining step rather than the hydrogen oxidation reaction (HOR). As shown in Figure 2-1, the ORR chemisorption energy vs. cell potential produces a volcano shaped curve having pure platinum on the extreme left (with the lowest ΔE_0) and all the other bimetallic metals are on the right side of the volcano (with

higher ΔE_0). For metals on the left side of the volcano, it indicates that oxygen atoms are binding too strongly and the catalytic rate is limited by the removal of adsorbed O and OH species. When adsorption is too strong, the surface will eventually be oxidized and become un-reactive. [9] On the other hand, for metals on the right side of the volcano, the oxygen atoms are binding too weakly with a slow transfer of electrons to adsorb oxygen. Hence the rate is limited by the dissociation of O_2. According to this model, the ideal catalyst would have oxygen chemisorption energy close to the peak of the volcano. With such catalyst, the activity would be maximized with a balanced rate of oxygen adsorption and desorption. [10] This model concludes that pure platinum is binding oxygen a little too strongly, and by compressing the unit cell with a 3d transition metal, the alloyed surface would form a weaker bond to oxygen, giving a higher activity.
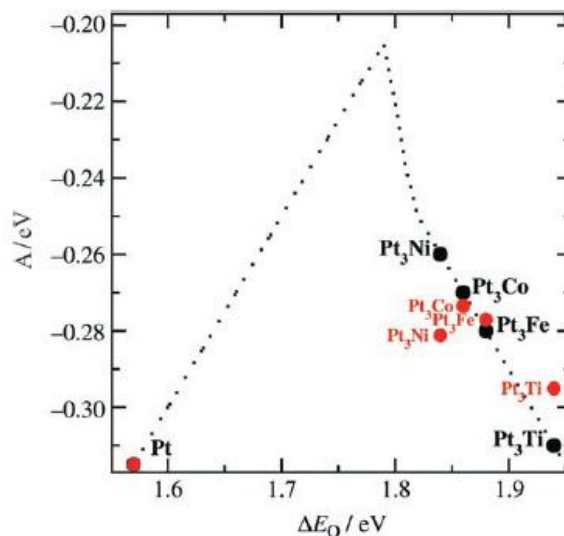
FIGURE 2-1 MODEL OF CATALYTIC ACTIVITY VS OXYGEN CHEMISORPTION ENERGY OF VARIOUS PT ALLOYS [9]

Specifically, alloying elements in platinum modify the electronic configuration by shifting the d band center downwards away from the Fermi level as shown in Figure 2-2. The oxygen and metals bond by coupling the oxygen 2p states with the metal d states. For a metallic environment, the filling of the bonding and anti-bonding states depends on the relative position of the Fermi level. The downward shift of the d states would result in more filling in the anti-bonding state hence a relatively weaker bond. In other words, the downward shift of the 5d band structure is attributed to the induced strain on the catalyst crystal which makes platinum alloy an ideal candidate to be used for fuel cell catalysts. [3], [9], [11], [12]
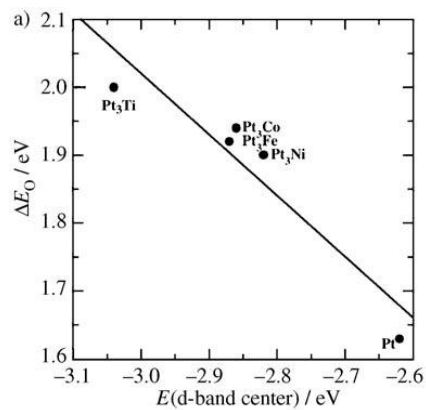
FIGURE 2-2 CORRELATION BETWEEN D-BAND CENTER AND OXYGEN ADSORPTION ENERGY OF VARIOUS PT ALLOYS [9]

2.2. SURFACES OF CATALYTIC NANOPARTICLES

With the knowledge that platinum alloys produce a higher catalytic activity than pure platinum, the next step is to tune the surface morphology of the platinum alloys to

maximize the performance. The key to catalytic activity improvement is to understand the structure of active sites on the surface of the nanoparticles. [13] In general, high Miller index planes exhibit higher catalytic activity compared with low Miller index surfaces. The reason is because high Miller index planes contain a greater density of atomic steps, ledges, and kinks which serves as active sites for breaking the absorbent's bond. [14] However, cubic nanocrystals typically facet at low indexed surfaces including (111), (110}, and (100} due to the fact that they are more stable. DFT calculations have been done to understand the absorption of oxygen onto these low index surfaces and thus it has been discovered that all these planes are stable sites for oxygen and specifically, that the (111) surface is the most active and stable.[15] Different facets yielding different activities can be explained by the variance of surface energies and energy bands associated with different planes. In general, the (111) plane has the lowest surface energy followed by (100) then (110).[14] Gu *et. al.* [16] performed density functional theory calculations on oxygen absorption on platinum surfaces. On the surface of the platinum, there are a number of different adsorption sites that oxygen could bind to as shown in Figure 2-3. Aside from the surfaces, it is possible for oxygen atoms to be absorbed inside the subsurface within one monolayer below the surface.
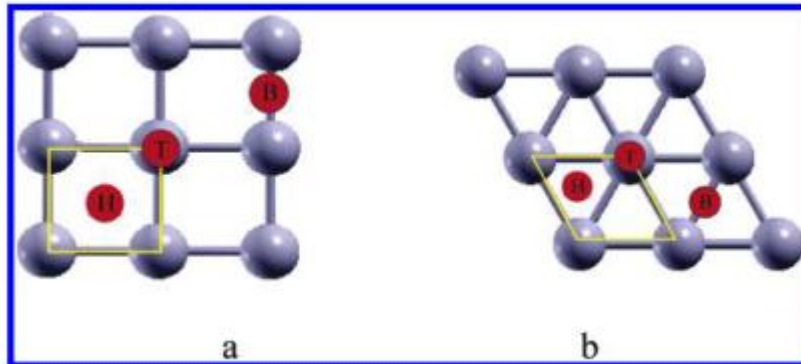
FIGURE 2-3 OXYGEN ADSORPTION SITES ON (001) AND (111) SURFACE OF PLATINUM. H, T, AND B DENOTES HOLLOW, TOP, AND BRIDGE SITES RESPECTIVELY

2.3. MICROSCOPY CHARACTERIZATION ON CATALYSTS

A number of microscopy techniques have been performed on catalysts to have a better understanding of their physical and chemical properties. It is known that nanostructures with different shapes and sizes exhibit unique properties; hence it is important to be able to characterize them on the nano-scale to understand the structure of these materials. In addition, the structure and composition of prepared catalysts is known to change under real fuel cell operation conditions. As a result, the study of catalysts degradation has attracted a lot of attention in recent years. However, many of the previous studies involved bulk system analysis of the catalysts and provides no insight on the atomic scale. Consequently, the usage of transmission electron microscopy is beneficial in the study of the nanoparticles. TEM imaging reveals the structures and morphology of the particles whereas techniques including EDX and EELS would resolve the composition information of the catalyst. TEM is not only capable of

9

allowing the understanding of the morphological and compositional information, but also the understanding of the degradation mechanism down to the atomic level by observing the change in morphology and composition at high resolution.

2.3.1. CATALYST MORPHOLOGY

One of the research objectives in catalyst synthesis is to be able to control the morphology of the nanoparticles. Physical properties including particle size, shape, and dimensionality would all affect the performance of the catalyst. Over the years, nanostructures with different shapes and sizes were synthesized and compared to achieve the highest catalytic activity along with a precise morphology control method. It is important to understand that electro-catalytic reactions occur on the surface of the catalysts, hence the activity of the reaction strongly depends on the surface of the catalyst. To maximize this interaction, the use of nanoparticles is highly beneficial as it maximizes the surface area to volume ratio, allowing more active sites to be used. With the miniaturization of catalysts, electron microscopy plays a key role in the study of the nano-structured catalysts. [17–19]

Nanoparticle synthesis commonly results in sphere-like shaped catalysts due to the natural phenomenon of decreasing surface energy to achieve a thermodynamically stable state. However, it is possible to synthesize non- spherically shaped catalysts including nanocubes, tripods, and, nanowires. [1] It is known that nanostructure with

different shapes exhibit unique chemical and physical properties, hence transmission electron microscopy is an unavoidable tool to characterize these nano-materials. Figure 2-4 below illustrates the different routes of synthesis of platinum nanocubes resulting in slightly different overall morphology revealed by electron microscopy. With the qualitative information of catalyst morphology, it is then possible to understand the roles of various key parameters in particle synthesis thus producing the desired nanoparticle structure. For example, it was learned that capping agents such as polyvinyl-pyridine (PVP) interact strongly with the metal surface and would block a significant number of active sites. This would be a procedure that is undesirable and should be avoided [20].
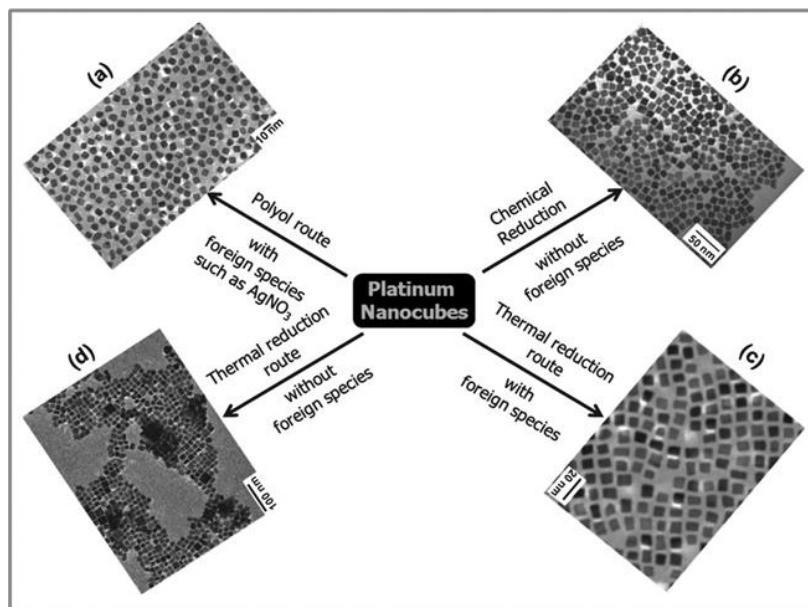
FIGURE 2-4 TEM MICROGRAPHS OF DIFFERENT PT NANOCUBES SYNTHESIZED BY DIFFERENT METHODS [1]

2.3.2. SUPPORTING MATERIAL

Aside from the nano-structured catalysts, the TEM has been widely used to study the supporting material as well. In order for these catalysts to be utilized in a fuel cell electrode, they must be supported on a conductive supporting material. Carbon is the most common and promising choice due to its high conductivity and large surface area properties. Figure 2-5 below shows a typical commercially available carbon support for platinum based catalysts. As shown in the figure, the cloud like shaped structures are the carbon and the black dots are the platinum [21]. Evidently, the nanoparticles can be heavily distributed on the support to maximize the contact surface area for ORR. In terms of catalyst support design, engineers are aiming to achieve a support with high surface area, high conductivity, and low degradation [22].
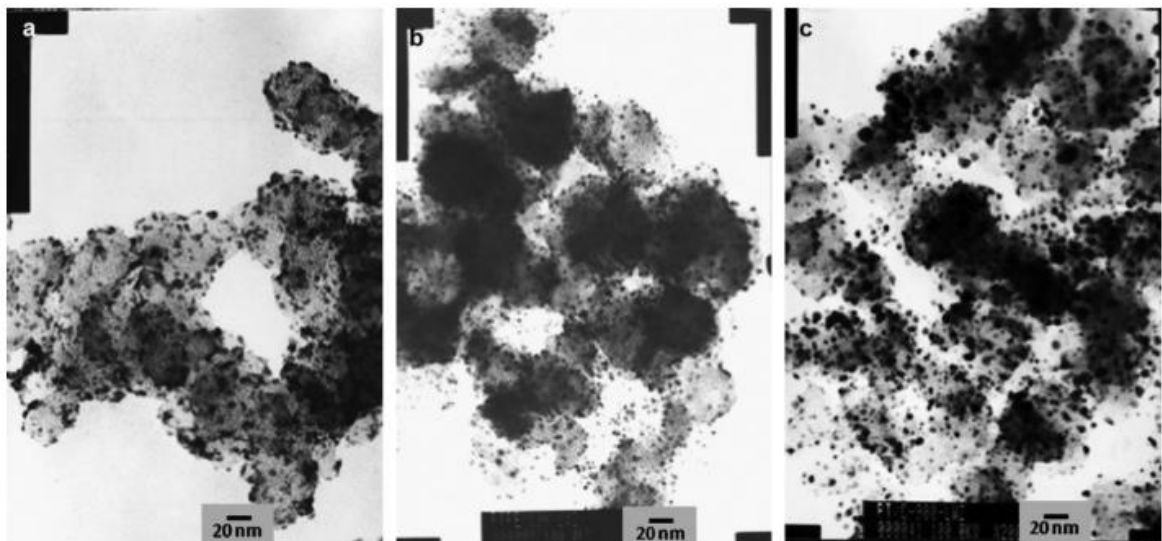
FIGURE 2-5 TEM IMAGES OF TYPICAL CARBON SUPPORTED PLATINUM NANOPARTICLES [21]

2.3.3. CORE- SHELL STRUCTURES

A strategic approach in platinum reduction is to synthesize core shell structures with a platinum rich surface. The reason is because all the catalytic reactions occur on the surface of the particles, thus a core-shell structure would minimize the amount of platinum being used, while maximizing the number of active sites on the surface. To confirm such unique structures, transmission electron microscopy techniques including high angle annular dark field (HAADF) imaging and energy dispersive x rays spectroscopy (EDXS) are often utilized to characterize the materials.

Peng et al. [23] utilized these techniques and discovered an electrochemical approach to produce nanostructures with platinum rich surfaces. The synthesis process involves the removal of Ag from PtAg nanoparticles through electrochemical treatment as shown in Figure 2-6. This dealloying process is favourable due to the large difference in standard reduction potential between the two metals. By experimenting with the electrochemical treatments at different potentials, they realized the potential has a direct influence on the particle size and composition as summarized in the schematic illustration below. With a low potential of 0.6V, little Ag dissolution occurred. The platinum rich surface started to form when the potential is 1.0V and above. They hypothesized that under high voltages, the exposed platinum atoms arrangement is reconstructed upon the dissolution of Ag, resulting in a platinum rich surface with a reduced diameter. To further confirm the platinum rich surface, EDXS spot analysis and line scans were performed as shown in the following images. It was concluded that after

high potential cycling, there is an increase in platinum concentration with a weak Ag

signal in the surface region of the particles, indicating a core shell structure.

Chen et al. [24] produced core shell structures but with a slightly different

approach. Prior to the electrochemical cycling, the particles were leached in an acid,

dissolving the non- noble metal and revealing a platinum skeleton. During the

electrochemical treatment, platinum atoms from smaller particles would diffuse to the

platinum skeletons, resulting in a core shell structure. However, unlike the previous

study by Peng et al. [23], there is an overall increase in particle diameter after the

cycling process. Similarly, Chen [24] performed EDXS line scans and provided a stronger

evidence of platinum rich surface as illustrated in Figure 2-7.

14
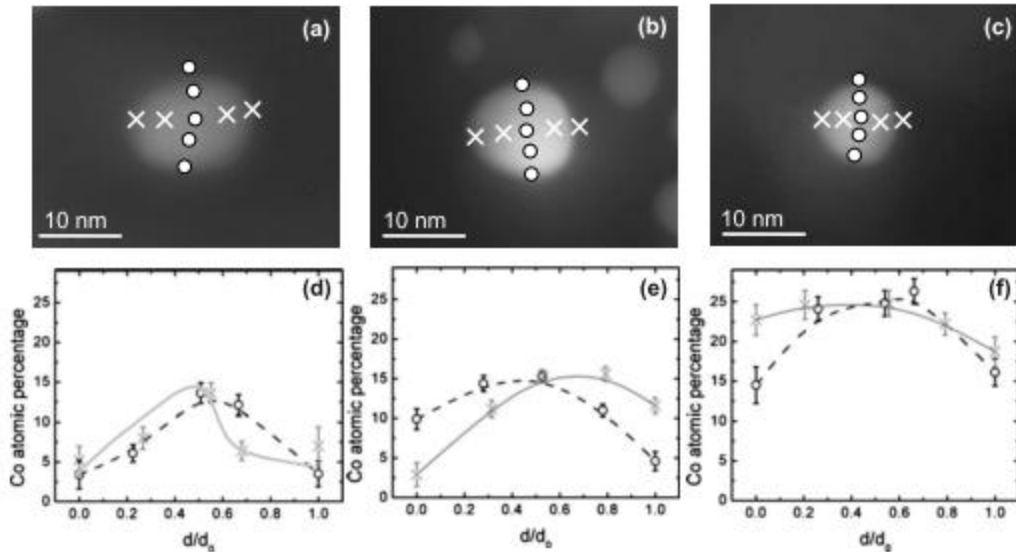
FIGURE 2-7 EDX LINE SCANS SHOWING CORE SHELL STRUCTURES OF PT RICH SURFACES IN TWO PERPENDICULAR DIRECTIONS (X AND CIRCLES). ALL THREE PARTICLES SHOW HIGHER CO CONCENTRATION IN THE CENTER IN BOTH DIRECTIONS [24]

Three particles approximately 10nm in diameter were subjected to EDX point analysis to determine the atomic composition at various locations of the nanoparticles. Two line scan with directions perpendicular to each other were performed on each particle as shown in Figure 2-7 marked by "X" and circles. Note that the TEM images obtained for EDXS are Annual dark field (ADF) images. The plots below each image give the Co atomic distribution across the relative location of the particle. All three nanoparticles give a parabolic distribution and the Co atomic concentration is maximal at the center of the particle. It is clear that the Co concentration at the particle edge is much lower than that of the center. However, the concentration of Co particle varies by particles as insert c Figure 2-7 shows a much higher Co atomic percentage compared to

insert a and b. If this postulated Pt-Co reconstruction is true and reliable, it may greatly

decrease the loading of Pt while maintaining high activity for the catalyst. [24]

The EDXS could also be used for compositional studies with more complicated

structures including multimetalic $Ag/FePt_3$ and Ag/Au as performed by Wang et. al. [25],

[26]. The main reason to synthesize particles with an Au core and $FePt_3$ is the increase in

particle stability and durability. It has been shown that multimetallic $Au/FePt_3$ not only

produces a higher activity, but also superior durability in terms of carbon monoxide (CO)

tolerance.   Gold acts as a stabilizer for the particle as is electrochemically inactive for

the ORR and iron is added to induce catalytic enhancements. Figure 2-8 below illustrates

the elemental distribution of the structure of the nanoparticle done by EDX.
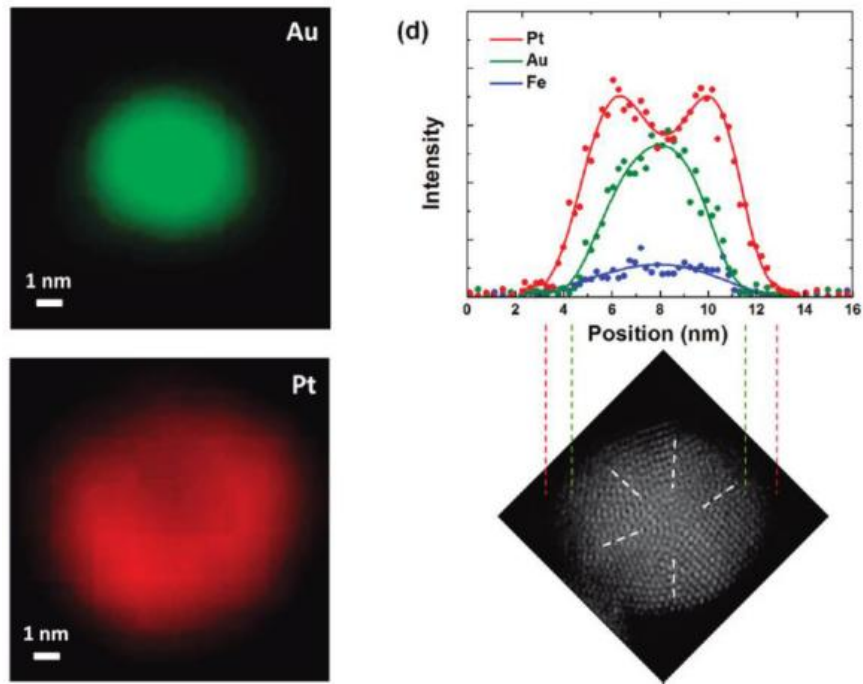
FIGURE 2-8 EDX ELEMENTAL MAPPING AND LINE SCANS PROVIDING EVIDENCE OF CORE SHELL STRUCTURE [25]

Another technique to confirm a core shell structure would be high angle annular dark field imaging. This imaging technique produces a Z contrast image in which if the atomic number of the two metals differs, they would produce a difference in intensity from regions with low Z as compared to regions with high Z. [12], [27] Figure 2-9 below illustrates Pt-Pd particles with brighter shells which indicates the presence of a platinum rich surface. However, the information provided by HAADF imaging is generally qualitative and thus cannot give an exact confirmation of the thickness of the platinum surface.
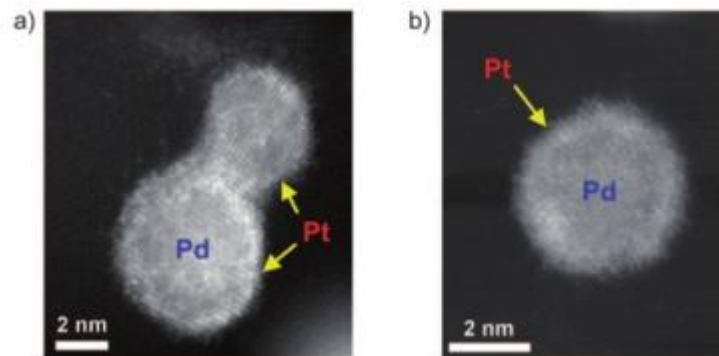
FIGURE 2-9 HAADF IMAGES OF SMALL PARTICLES SHOWING PT MONOLAYER SHELL ON A PD CORE [27]

2.3.4. IDENTICAL LOCATION-TEM

In the work performed by Mayrhofer et al.[28–30], they specifically used transmission electron microscopy to study the morphological change of a platinum catalyst under electrochemical treatment. They have introduced a novel and innovative method to study the treated catalyst with a technique called identical location transmission electron microscopy (IL-TEM). In summary, after the initial TEM imaging of the as prepared particles on the copper grid, the grid was then removed and directly subjected to potential cycling based on a typical lab scale electrochemical treatment setup. This was followed by another TEM imaging process on the same grid that has been potentially cycled. This enables researchers to study the same location of the sample before and after electrochemical treatment.

18
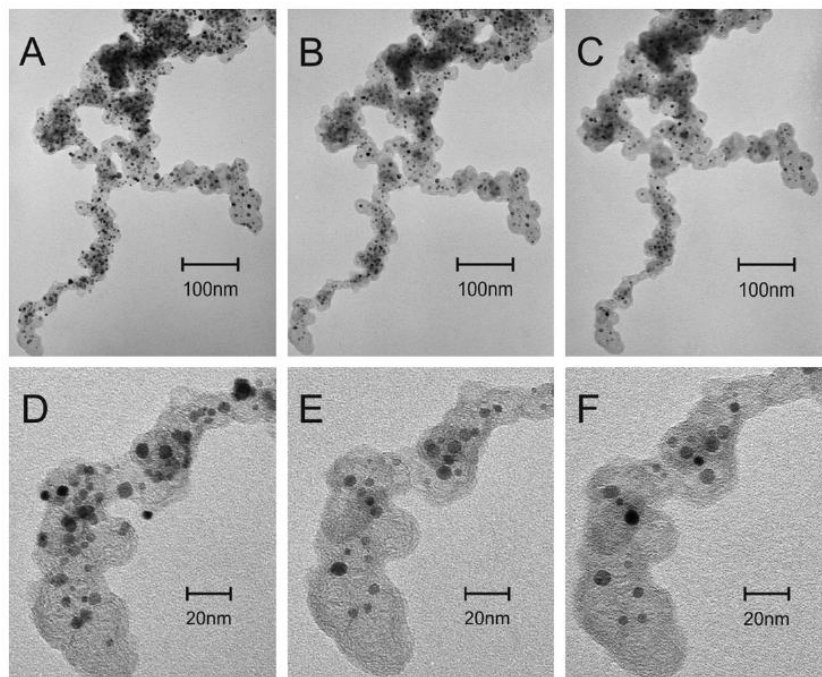
FIGURE 2-10 TEM IMAGES OF PT ON CARBON SUPPORT OF THE EXACT SAME LOCATION BEFORE AND AFTER ELECTROCHEMICAL TREATMENT. A & D PRIOR CYCLING, B & E AFTER 2 HOURS OF CYCLING, AND C & F AFTER 4 HOURS OF CYCLING [28]

The IL-TEM method was conducted with JEOL, JEM 100CX TEM, with a beam energy of 100 kV on platinum nanoparticles. Different bright field images of the catalyst were taken before, after 2 hours, and after 4 hours of electrochemical treatment. Distinctive shapes of the carbon supporting material were identified and the images of treated and non-treated samples were compared as demonstrated in Figure 2-10 above. Figure 2-10 insert A, B and C displays the platinum particles prior to the treatment, after 2 hours of treatment, and after 4 hours of treatment respectively. All images were taken at the same location with the same magnification. D, E, and F correspond to the lower left corner of the immediate image above at a higher magnification. From the images of A to C, it is evident that

there is a decrease in the number of black dots (i.e. the nanoparticles) following an increase in the cycle time. These results are more obvious in images D to E where there is a significant decrease in particles comparing inserts D and E. Figure 2-11 illustrates the particle size distribution obtained from the TEM micrographs. Quantitatively, the number of particles decreases to 71% after the initial 2 hour treatment (insert B) and further decreases to 47% after 2 additional hours of treatment (insert C). Mayrhofer calculated the average particle size and see that there is only a slight increase in diameter from 4.9 to 5.6nm from A to C with a decrease in total area of particles on the same carbon support. This suggests that both Oswald ripening and particle coalescence play only a minor role in these conditions; it is evident that the detachment of the nanoparticles from the caron support onto the electrolyte is the predominant degradation mechanism.
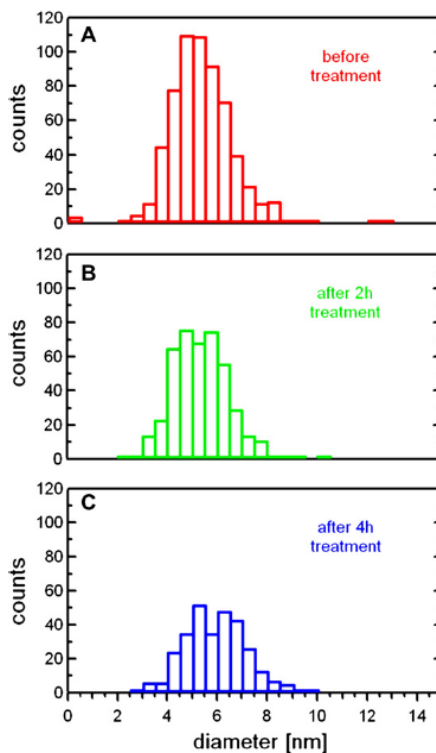
FIGURE 2-11 SIZE DISTRIBUTION OF PT NANOPARTICLES AFTER CYCLING DONE BY IL-TEM [28]

IL-TEM is a novel method to study the degradation and morphology of the catalysts as it gives absolute information by studying the same location. However, it should be mentioned that this is a tedious and lengthy process as it can be extremely difficult to find the exact location after performing electrochemical cycling on the copper grid.

The chemical ordering of the catalytic nanoparticles is an important factor to consider as it is known that ordered crystals will exhibit a higher activity than disordered crystals. The ordering and disordering mentioned refers to the arrangement of atoms in a crystal. Simply, when something is arranged in a repeatable pattern, it would be classified as ordered. On the other hand, when matters are arranged on a lattice randomly without specific patterns it would be disordered as shown in Figure 2-12 below. However, as it is difficult to classify a material as completely ordered or disordered, a more appropriate term is the "degree of ordering".
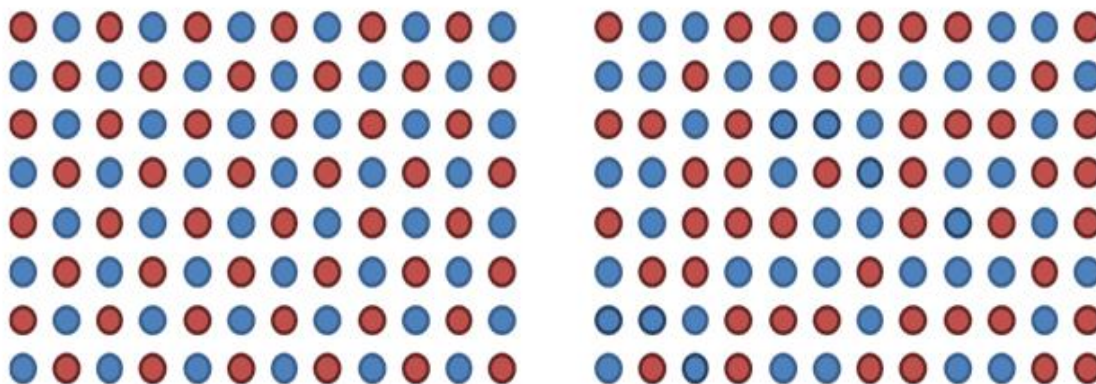
FIGURE 2-12 ILLUSTRATION OF ORDERED AND DISORDERED CRYSTALS. (LEFT- ORDERED CRYSTAL SHOWING REPEATABLE PATTERNS; RIGHT - DISORDERED CRYSTAL WITH RANDOM ARRANGEMENTS)

It is possible by means of change in temperature for a crystal to transform from the ordered to disordered state. The general trend for bulk material is that as temperature increases, ordering decreases. The reason scientists and researchers are

interested in chemical ordering is that the arrangement of the atoms would greatly affect the performance of the materials. For example in the field of electrocatalysts, ordered alloys exhibit much greater activity than disordered alloys. All in all, being able to control the ordering of a crystal would greatly enhance its performance for various applications.

2.4.1.   ORDERING FOR BULK PT-FE

Figure 2-13 below is a well studied phase diagram for bulk Pt-Fe crystal. As presented, there are two different ordered phases for Pt-Fe with three different crystal configurations including $L1_2$ (Fe_3Pt, Pt_3Fe) and $L1_0$ (PtFe). $L1_0$ and $L1_2$ are both ordered crystal with tetragonal and cubic unit cells respectively. At low temperatures, the bulk crystal remains in the ordered state. This is due to the negative enthalpy of mixing, in which atoms are likely to bind to unlike atoms, forming the repeatable ordering. At high temperature, the ordered $L1_0$ and $L1_2$ states would transform to the disordered A1 state.
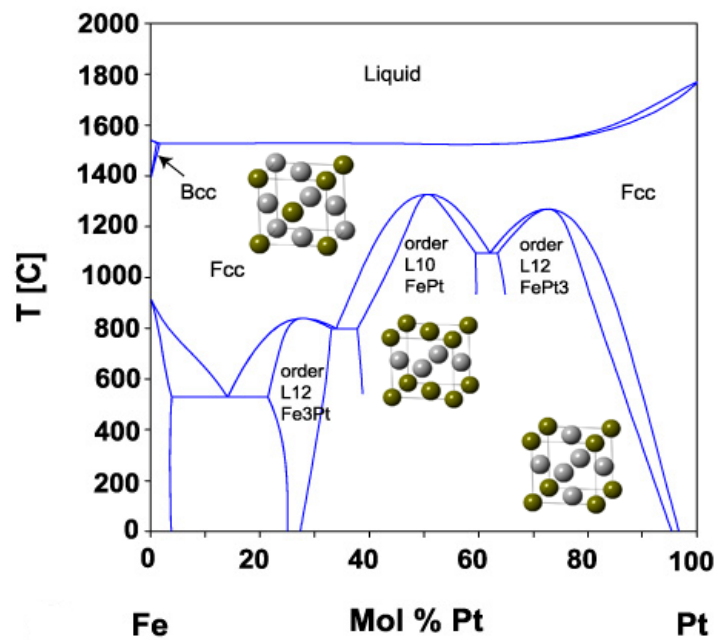
FIGURE 2-13 PHASE DIAGRAM OF PT-FE

2.4.2. ORDERING PARAMETER

To quantify the degree of ordering, a value known as the ordering parameter can be used. Imagine a completely ordered binary crystal where each atomic position is occupying one type of atoms only, then the ordering parameter for this fully ordered crystal would be 1. The following equation describes the ordering parameter. $\eta_s = [N_1(1) - N_1(2)]/[N_1(1)+N_1(2)]$ Where $N_1(1)$ is the number of type 1 atom in position 1, and so on. As presented, the denominator is the total number of atoms in the crystal hence the ordering parameter is a value ranging from 0 to 1, where 0 means a completely disordered crystal.

24

When plotting the ordering parameter with temperature, ordering decreases to its minimum when a critical temperature is reached as shown in Figure 2-14. In general, when a crystal with ordering is heated, more and more atoms would occupy the "incorrect" positions, and ordering would eventually disappear. This transformation indicates that the thermal motion overcomes the tendency of atoms towards long range ordering.
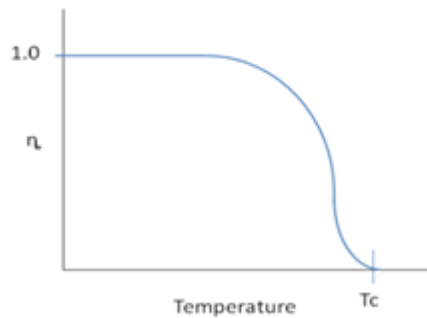
FIGURE 2-14 SKETCH OF ORDERING PARAMETER VS TEMPERATURE FOR BULK MATERIALS

2.4.3. ORDERING FOR NANOPARTICLES

As mentioned earlier for bulk crystals, the degree of ordering decreases as temperature increases. However this trend does not apply to nanoparticles. The reason being that nanoparticles are synthesized at room temperature and are predominately disordered. During the synthesis process, the growth kinetics are much faster than the ordering kinetics and they would remain in the metastable disordered state. A post annealing process at high temperature is required to transform these nanoparticles

from the initial A1 state to the ordered state. For clarification, critical temperature (Tc) refers to the transformation from order to disorder. Whereas annealing temperature (Ta) refers to the transformation from disorder to order.

Endo. et. al. [31] explored the structure characteristics of as prepared Pt-Fe as a function of different post annealing temperatures. With the disordered Pt-Fe nanoparticles, different sample batches were annealed at different temperature, and XRD was performed to detect the superstructure reflections to determine the ordering.
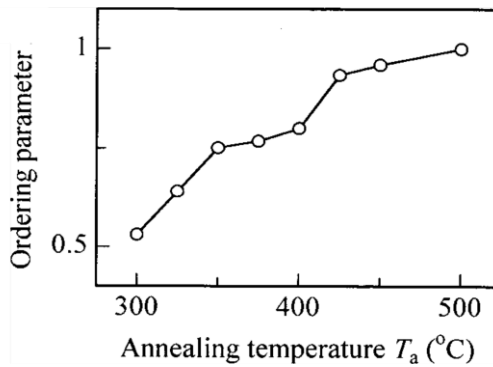
FIGURE 2-15 ORDERING PARAMETER VS ANNEALING TEMPERATURE FOR NANOPARTICLES [31]

The results indicate that as the annealing temperature increases, the ordering parameter increases as well as illustrated in Figure 2-15. Between the temperature of 300°C and 425°C, he referred to the nanoparticles as being partially ordered since the ordering parameter is between 0.5 to 0.75. When the temperature is above 425°C, the ordering parameter is approaching 1 which indicates a fully ordered phase.

26

2.4.4. TEM IN-SITU EXPERIMENT TO DETERMINE ORDERING

Another group of researchers, Alloyeau et. al. [32] performed an in-situ TEM experiment to understand the ordering effect on temperature with Pt-Co nanoparticles. Similarly, the synthesized particles are in the disordered A1 state and because they are described as non equilibrium structures, they cannot be explained with a phase diagram. For their experiment, a heating specimen holder is used to heat the sample inside the TEM that is capable of reaching 1000$^\mathrm{o}$C. The diffraction pattern is observed to determine the ordering of the nanoparticles. Prior to the in-situ experiment, a correlation between the composition and the lattice parameter of disordered nanoparticles was performed. The compositional information was obtained by EDX whereas the lattice parameter was obtained by the electron diffraction measurement. With the correlations made, the deduction of composition of the disordered nanoparticles is possible by measuring the lattice parameter by the diffraction pattern as shown in Figure 2-16.
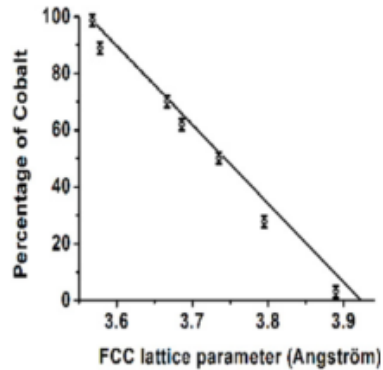
FIGURE 2-16 CORRELATION BETWEEN CO CONCENTRATION AND LATTICE PARAMETER [32]

Starting at room temperature, the sample is first heated to 600°C. Then increasing by small increments of 30°C until the temperature reached 700°C, then in smaller increments up to 850°C. After maintaining at a high temperature of 850°C for 30 mins, the temperature is then decreased to test the reversibility.

As mentioned earlier, the detection of superstructure reflections was used to determine the ordering of the nanoparticles. In general, diffraction patterns display two kinds of reflections: fundamental and superstructure. Consider reflections hkl. hkl would have the same parity for a fundamental reflection (ex/ 002, 111, 220). On the other hand, superstructure reflections are chemical sensitive reflections that are forbidden in disordered structures. For reflections hkl, h and k would have the same parity that is different of l for a superstructure reflection. Quite often superstructure reflections are a set of weaker diffraction spots between fundamental reflections.

Figure 2-17- left below is the results for the in-situ experiment. Starting at room temperature, only the fundamental rings were observed. At approximately 570°C, the

superstructure ring of 001 starts to appear, and becoming visible at 600°C. As the temperature gradually increases, the superstructure reflections then increase in intensity and the diffused ring becomes a sharp one. The sharp intensified ring lasts until 770°C is reached, whereby the superstructure rings start to disappear. Heating goes until 850°C and the particles remain disordered. To test the reversibility, the temperature is then lowered from 850°C. Superstructure reflections start to appear again at 715°C, remaining visible even when the temperature is returned to room temperature. Figure 2-17-right is a summary of the in-situ experiment where the red and blue regions show the disordered and ordered state respectively.
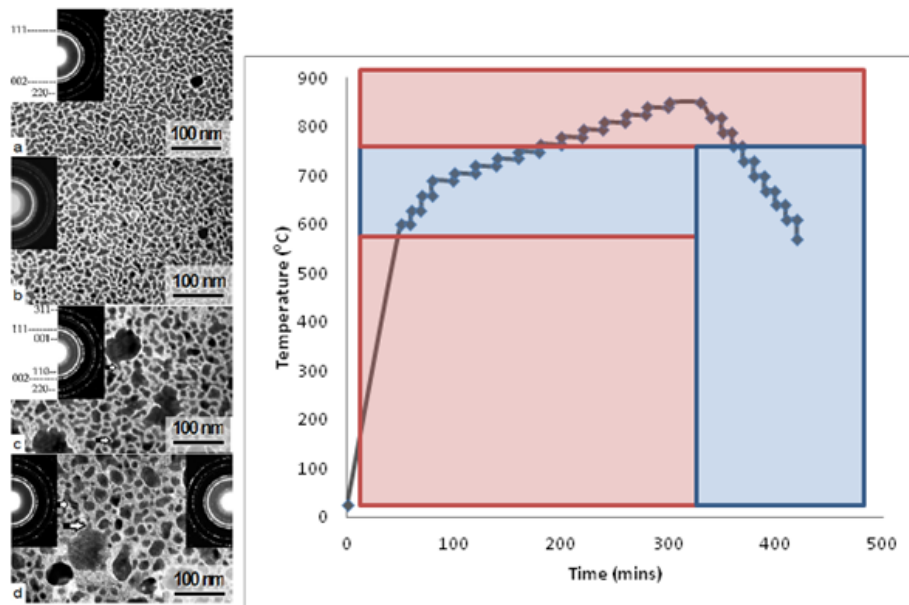
FIGURE 2-17 LEFT- TEM IMAGES OF NANOPARTICLES DURING INSITU HEATING. INSERTS SHOW DIFFRACTION PATTERNS AS EVIDENCE OF ORDERING; RIGHT- HEATING PROFILE OF INSITU EXPERIMENT, RED AND BLUE REGION INDICATES DISORDERED AND ORDERED REGIONS RESPECTIVELY [32]

The in-situ experiment results agree with the ordering effect as expected. Starting at room temperature, the nanoparticles are disordered until an annealing temperature of around 600$^\text{o}$C. The degree of ordering then increases until the critical temperature of 770$^\text{o}$C is reached when the L1$_0$ state is transformed to the A1 disordered state. This process however is reversible as the temperature is lowered to room temperature, the nanoparticles returned to their ordered state. As presented, the order to disorder transition for nanoparticles are similar to bulk except it is at a much lower (770$^\text{o}$C) temperature than bulk (850$^\text{o}$C). With this experiment, Alloyeau concluded that 650$^\text{o}$C is an appropriate annealing temperature for Pt-Co nanoparticles to achieve ordering. [32]

2.4.5. ORDERING VS PARTICLE SIZE

The same group of researches performed a STEM nano probe diffraction (NPD) to determine the ordering of individual nanoparticles. By maintaining a parallel beam, nano probe diffraction gives structure and orientation of single particles rather than the sample as a whole. The benefit of nano probe diffraction is that lens aberration does not affect the intensity of the diffraction spots, whereas aberration induced deformation can occur for HRTEM. Similar to the previous techniques, the diffraction patterns are analyzed. [33]

With a post annealing temperature of 650°C, ordering was expected for each nanoparticle, but that is not the case. As shown in Figure 2-18 b and c below, both of these nanoparticles are oriented in the 111 direction. However, superstructure reflections are only detected for particle c and not particle b.

FIGURE 2-18 NANOPROBE DIFFRACTION OF INDIVIDUAL PT-CO NANOPARTICLES; B- NPD SHOWING FUNDAMENTAL REFLECTIONS; C- NPD SHOWING BOTH FUNDAMENTAL AND SUPERSTRUCTURE REFLECTIONS [33]

By probing hundreds of nanoparticles, it was found that superstructure reflections were not observed in all of them. One reason is due to the extinction rule. Consider reflections hkl, when h and k have a different parity, superstructure reflections would not be shown even if the particle is ordered. There is only a limited set of orientations that allow the determination of ordering without any ambiguity. In addition, ordering was never observed for particles as small as 3 nm no matter what orientation it is in. This indicates that particle size may influence the ordering behaviour as well.

Henceforth, Alloyeau further studied the size and shape effect on atomic ordering. At an annealing temperature of 650°C, no ordering can be observed for

31

particles smaller than 3nm. However, ordering can be achieved for small particles below

3nm when the annealing temperature is at 500°C. To understand this phenomenon, a

Monte Carlo simulation was performed to study the critical temperature of particles

with different sizes. With the nanoparticles created in their ordered state, the critical

temperature can be as low as 450°C for a 2nm diameter particle compared to the bulk

critical temperature of 850°C as shown in Figure 2-19 (left). This suggests that when

annealing at high temperatures, ordering may be achieved for the majority of the

particles, but it may go beyond the critical temperature of small particles, hence

resulting in their disordering. In another words, if there is a precise control in particle

size, it would be possible to control the ordering of individual nanoparticles. [33], [34]
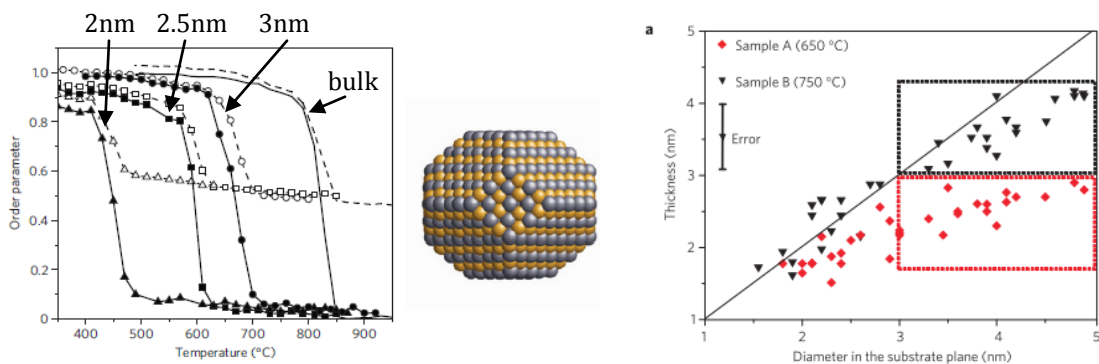
FIGURE 2-19 LEFT- SIMULATIONS SHOW A DECREASE IN CRITICAL TEMPERATURE AS PARTICLE SIZE DECREASES; RIGHT- CORRELATION PLOT OF PT-CO NANOPARTICLES THICKNESS AND THEIR DIAMETER [33]

In addition to the simulation, TEM tomography was also performed to study the

shape of the nanoparticles. A series of 2D TEM images were taken at different angles

and integrated to a 3D representation of the catalysts. With the reconstructed model,

slices of images can be made to reveal the thickness and shape of the nanoparticles. The

tomography results show that not all particles are sphere-like in shape, and particles annealed at 650°C are flatter than the ones annealed at 750°C. (these particles are not spherical due to the synthesis method) Figure 2-19 (right) correlates the particle thickness with diameter. Even for particles with diameter greater than 3nm (as shown in the red rectangle), ordering may not be observed since the thickness is small. They concluded that the size effect on the critical temperature is uniquely determined by the smallest characteristic length on the nanoparticle. Therefore, for particles annealed at 650°C, even if the particle diameter is larger than 3nm, it may still be disordered because the particle thickness is below 3nm. [33]

2.4.6. KINETICS OF ORDERING FOR NANOPARTICLE

The ordering effect of nanoparticles can be explained by kinetics. The equation below describes the volume diffusion of atoms within a nanoparticle. Where λ is the diffusion length, D is the diffusion coefficient, t is the time, D_0 is the pre-exponential factor, E_A is the activation energy, k is the Boltzmann constant, and T is the temperature. The values of platinum were chosen for simplicity since it is the least diffusing component of the alloy.

$$\lambda = \sqrt{Dt} = \sqrt{D_0 \exp\left(\frac{-E_A}{kT}\right)t}$$

With this equation, three different temperature scenario calculations were performed. At room temperature with a time of 1 hour, the mean diffusion length is 1.565 x 10^{-25} m which is much smaller than the nearest atom distances. Therefore, at room temperature, the disordered nanoparticles would remain disordered. When the temperature is increased to 525 C for one hour, the mean diffusion length is calculated to be 0.3 nm which is approximately the distance of the nearby atom. With this temperature, the atoms have enough energy to jump from the current meta-stable site to a more stable site, thus achieving ordering. If we further increase the temperature to 800°C, the calculated diffusion length becomes really large such that the atoms may jump to other sites, hence resulting in the A1 disordered state again. As presented, atomic diffusion is dependent on both time and temperature. However, this is a simplified equation that does not take surface diffusion, particle size, and environment into account. [35]

In summary, the synthesized nanoparticles are predominately disordered. Annealing at high temperature is required to achieve ordering, but must remain under the critical temperature to avoid the order – disorder transition. Techniques including in-situ TEM, XRD, and nanoprobe diffraction are used to detect the superstructure reflections. Lastly, critical temperatures still exist for nanoparticles but it is much lower than that of bulk. In general, the smaller the particle size, the lower the critical temperature.

3. OBJECTIVE

The objective of this project is to study the morphology and composition of catalytic nanoparticles using transmission electron microscopy. Being able to understand these nanoparticles down to the atomic scale would greatly contribute to the development of catalysts and the design for the next generation fuel cell. Critical morphological and compositional information obtained include size distribution, surface structure, facets and crystal orientations, atomic ordering, elemental analysis, and degree of defects. Understanding all these factors could make it possible to tune the surface morphology of catalysts to maximize performance. In addition, the TEM is also utilized to study the change in structure and composition after electrochemical cycling. Platinum based catalysts were investigated including Pt-Fe and Pt-Co. The majority of the results presented in this paper are obtained by aberration corrected transmission electron microscopes, and techniques including HRTEM, HAADF, multi- slice simulations, EDX, and nano- probe diffractions were used. The ultimate goal is to maximize surface active sites with minimal usage of platinum. All the above mentioned factors can be adjusted by various synthesis approaches, but in order to do so, we must understand the materials by the means of microscopy.

4. EXPERIMENTAL METHODS

4.1. NANOPARTICLES PREPARATION

Two different nanoparticles were investigated namely Pt-Fe and Pt-Co. Both alloys were synthesized by our collaborator at the Institute of Chemical Processing and Environmental Technology (NRC) using a polyol method followed by a wet impregnation process. Firstly, the synthesis of Pt colloids was carried out by dissolving PtCl4 in ethylene glycol. Next, Vulcan XC-724R and Ketjen Black EC600JD carbon was added for Pt-Fe and Pt-Co samples respectively. The resultant carbon-supported Pt catalyst was then filtered, washed, and dried in an air oven. Lastly, for the wet impregnation method, $Fe(NO_3)_3$ and $Co(NO_3)_3$ were added to the suspension of Pt-Fe and Pt-Co respectively. The particles were subsequently annealed in an H_2 enriched atmosphere at 800 ^{o}C to reach the chemically ordered phases. In order to study the stability of the catalysts, the catalyst layers were electrochemically treated for various potential cycles using an industry protocol. Electrochemical cycling are all done in O_2 saturated $HClO_4$ between 0 – 1.2V vs RHE with a sweep rate of 50 mVs^{-1}.

4.2. TEM ANALYSIS

Morphological and compositional characterization was mainly performed by two aberration-corrected FEI Titan 80-300 electron microscopes operated at 200 keV. In

addition to ultra high resolution imaging, high angle annular dark-field (HAADF) imaging and energy dispersive X-ray spectroscopy (EDXS) mapping were carried out. One of the instruments (FEI Titan 80-300 Cubed) is equipped with two aberration correctors (one of the probe-forming lens and one of the imaging lens) providing ultrahigh-resolution HAADF-scanning TEM (STEM) images, high-resolution phase contrast imaging (HRTEM), and an EDXS detector (Oxford Instruments Si-Li detector). The second instrument is equipped with an aberration-corrector of the image-forming lens for HRTEM and an EDXS detector (Oxford Instruments Si-Li detector).
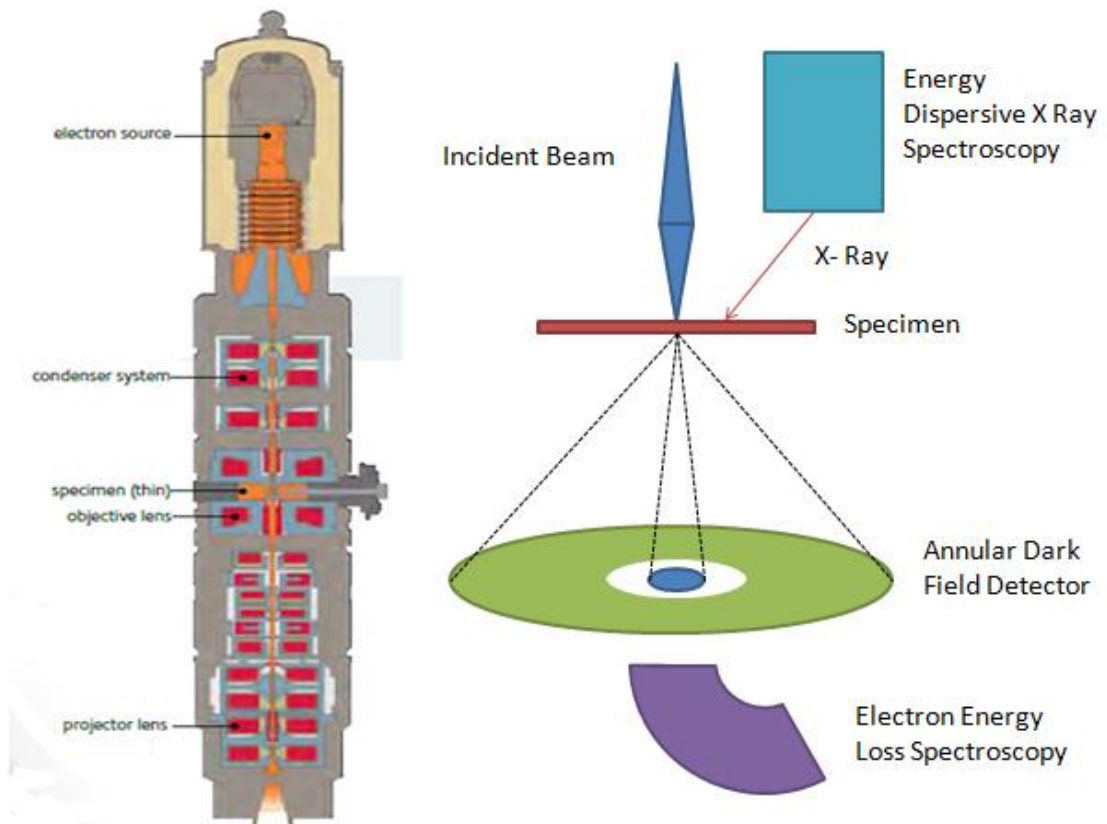
FIGURE 4-1 (LEFT)CROSS SECTION OF FEI TITAN TEM (OBTAINED FROM FEI.COM), (RIGHT) SCHEMATIC DIAGRAM OF STEM MODE

Figure 4-1 (left) illustrates the cross section of the major components of a TEM. In summary, the electron gun at the top provides the high-energy electron source. The electrons will pass through the condenser system which condenses the beam onto the thin specimen. The objective lenses then focus the electrons and magnify the image onto the fluorescent screen/ CCD camera. Figure 4-1 (right) shows a schematic diagram of scanning transmission electron microscopy. Particularly for the bimetallic alloy of interest, high angle annular dark field imaging is useful as it produces a Z contrast image. HAADF images are generated by integrating signals from electrons scattered at high scattering angles following Rutherford scattering. In these conditions the intensity is proportional to $Z^{1.6}$ where Z is the atomic number of the scattering atoms. As a result, HAADF imaging is the ideal tool for the study of particles, having elements with large Z differences. For elemental analysis, the EDXS detector is an attachment located above the specimen. X- rays would be bombarded onto the sample and an X-ray detector would collect the characteristic energy produced by the sample.

4.3. TEM SAMPLE PREPARATION

For catalyst samples prepared in powder form, the powders are first ground by glass slides before dry pressed onto a lacey carbon copper grid. For catalyst samples on carbon paper, two different methods were used to deposit the catalyst on the copper grid. The first method ultra-soncates the carbon paper in ethanol for two hours. The sonicated suspension should have a faint gray transparent colour to avoid a thick catalyst sample. Additional ethanol was added to dilute the suspension if the colour was too dark. The suspension was then drop cast onto the carbon grid and air dried for TEM

analysis. The second method is similar to the dry pressing method but the catalyst powders were first removed from the carbon paper by direct scraping. To avoid contamination in the microscope (mostly the formation of hydrocarbon film), samples that were prepared in ethanol were baked with the TEM holder in the vacuum at 70° C for two hours prior TEM analysis.

4.4.X- RAY DIFFRACTION

The X-ray diffraction patterns were obtained using a Bruker D8 Advance diffractometer with Brag- Brentano geometry with a Cu K alpha source. The collection angle ranges from 20° to 90° with a step size of 0.02^o and an acquisition time of 3 seconds per step.

5. EXPERIMENTAL RESULTS AND DISCUSSION

5.1.PT-FE CATALYST

A detailed structual characterization of Pt-Fe catalyst nanoparticles is carried out using aberration corrected and conventional transmission electron microscopy together with detailed interpretation of the images. 20wt% Pt/C precursor catalysts were first synthezised using a polyol method followed by a wet impregnation method with iron nitrate to produce Pt-Fe particles. The particles were subsequently annealed in an H_2 enriched atmosphere at 800ºC to reach the chemically ordered phases. In order to study the stability of the catalysts, the catalyst layers were electrochemically treated for 10,000 potential cycles using an industry protocol. This consisted of cycling at 50 mV/s between 0 and 1.2V vs RHE. Specifically, two different Pt-Fe stoichiometries were studied including Pt_3Fe and Pt_3Fe_2.

5.1.1. BRIGHT FIELD TRANSMISSION ELECTRON MICROSCOPY IMAGING

From TEM imaging nanoparticles of both compositions appear to be similar with no clear observable differences from simple inspection. Figure 5-1 shows a typical Vulcan carbon aggregate with Pt-Fe particles distributed randomly on the support as acquired by the Philips CM-12 conventional TEM.
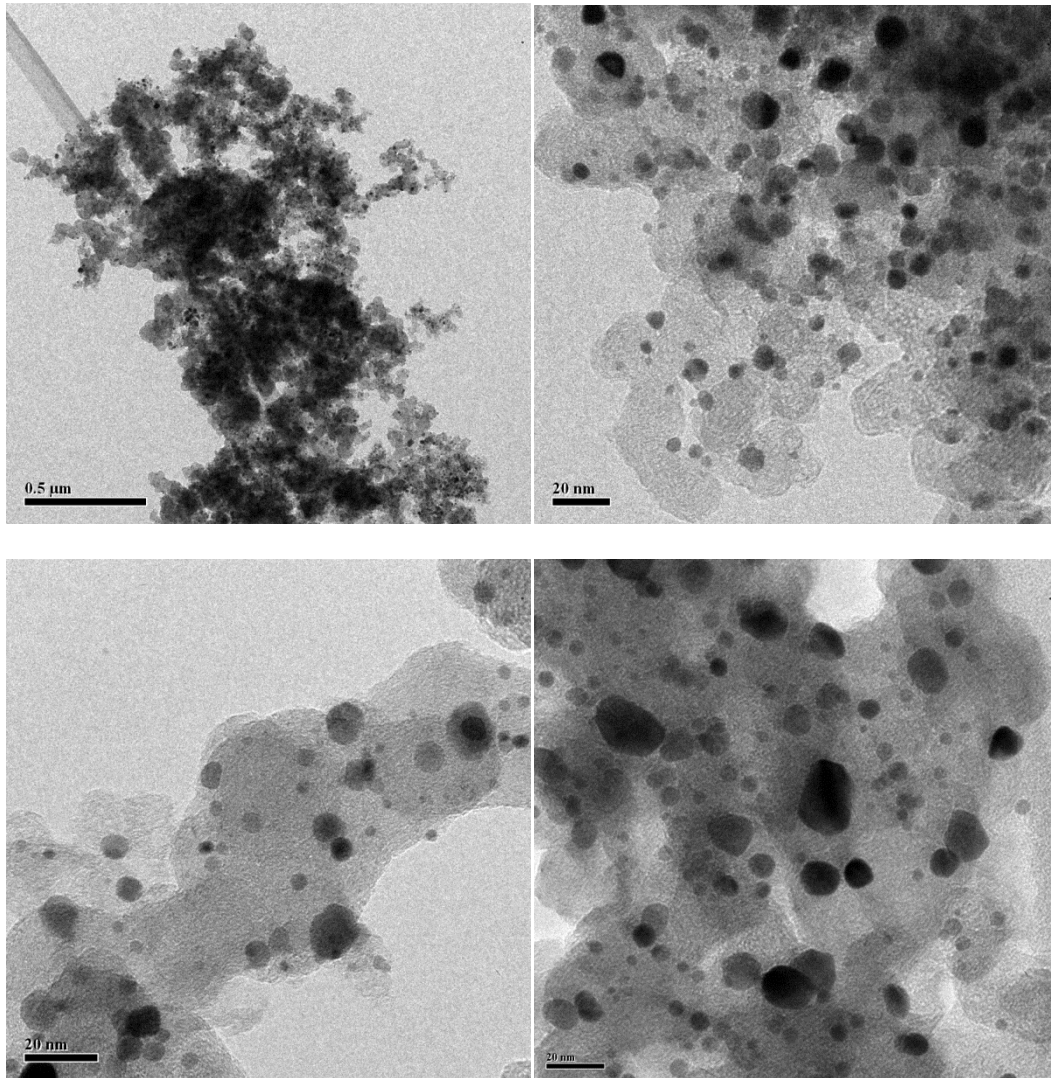
FIGURE 5-1 BRIGHT FIELD TEM IMAGES OF VULCAN SUPPORTED PT-FE NANOPARTICLES

As seen in Figure 5-1, the carbon supported nanoparticles have irregular shapes with a wide size distribution. The nanoparticles appear to be sphere-like in shape with some elongated truncated edges. The support produces the typical amorphous/ graphitic-like background contrast with the particles. The nanoparticles are randomly dispersed on the support with some areas more densely populated. High resolution transmission

41

electron microscopy (HRTEM) was also performed as shown in Figure 5-2. In HRTEM, small particles exhibit lattice fringes indicating the crystalline nature in particles even as small as 2nm (Figure 5-2 b). The uneven contrast and lattice shown on larger particles indicate the presence of overlapping nanoparticles (Figure 5-2 a).[23], [36]
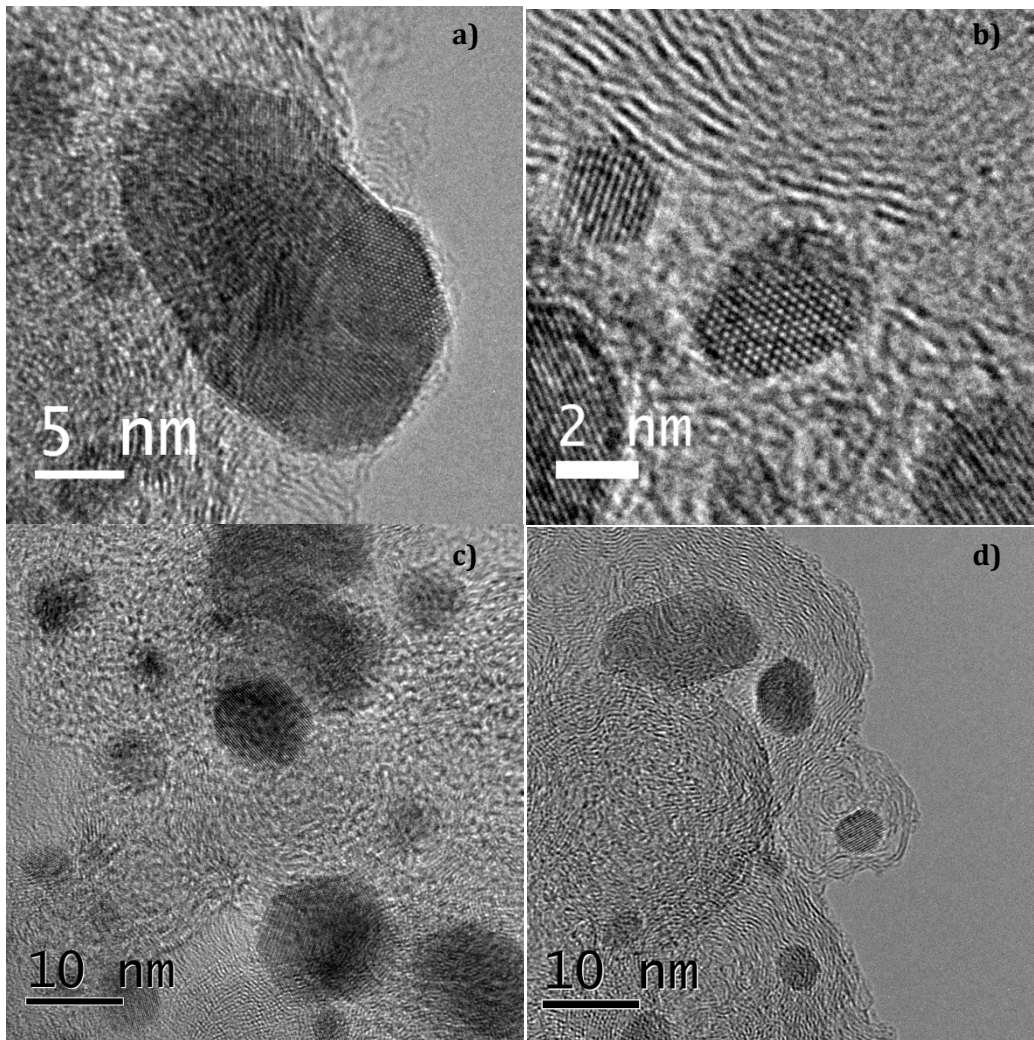
FIGURE 5-2 HRTEM IMAGES OF VULCAN SUPPORTED PT-FE NANOPARTICLES SHOWING LATTICE FRINGES AND ATOMIC COLUMNS

Both alloy compositions (Pt_3Fe and Pt_3Fe_2) exhibit a large size distribution ranging from 1 to 24 nm (Figure 5-3). Pt_3Fe peaked at 3nm both prior to and after cycling, whereas Pt_3Fe_2 peaked at 3 and 2 nm prior to and after cycling, respectively. Electrochemical treatment does not result in any obvious changes in particle shape and morphology, but the treatment of 10,000 cycles caused a change in particle size.
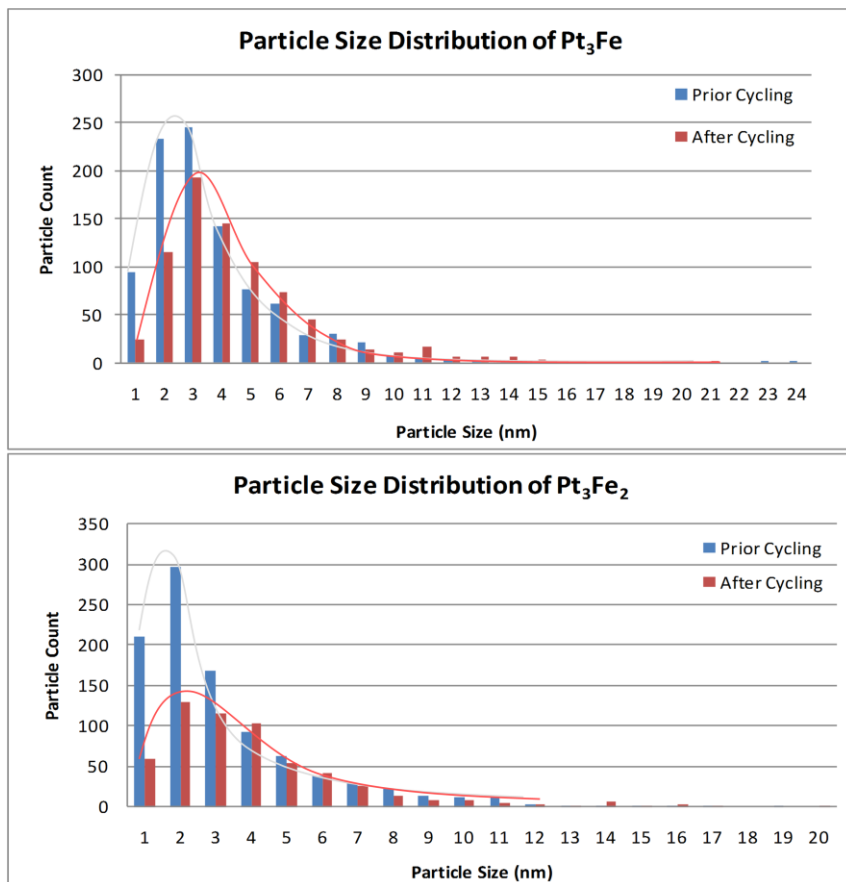
FIGURE 5-3 PARTICLE SIZE DISTRIBUTION OF PT-FE NANOPARTICLES

The calculated size averages of Pt_3Fe and Pt_3Fe_2 before and after electrochemical treatment are tabulated in Table 5-1. It is shown that the treatment causes an increase in the average particle size by approximately 1 nm in diameter and that this is consistent

for both compositions. The increase in diameter can be explained by the phenomena of Oswald ripening. Larger particles are more energetically stable than smaller particles, hence atoms would diffuse to larger particles to decrease surface energy.[24],[37],[38] Focusing on the lower size range between 1 to 5 nm for Pt_3Fe before cycling, we see that the curve is asymmetric and it peaks at 3 nm with the next highest peak at 2nm. However after cycling, we see that the curve skews to the left having the second highest peak at 4nm. This trend in size distribution matches with the Lifshitz- Slyozov- Wagner model and it is also evidence of Oswald ripening. [39] Consistent with literature, this asymmetric curve trend is also observable for Pt_3Fe_2. Furthermore, the broad diminishing spread on the size distribution curve in Figure 5-3 suggests particle migration and coalescence as it corresponds to a log normal distribution function.[25] Unlike Oswald ripening, coalescence involves the movement and merging of small crystals to form larger particles which most likely happened during the annealing treatment. Qualitatively, particle migration and coalescence was observed from our TEM examination where a small 2nm diameter particle was sintered with a 12nm diameter particle as shown in Figure 5-4. In addition, there is also a significant decrease in particle count for the samples that were electrochemchemically cycled. This could suggest that the particles are falling off the carbon support as deduced by Mayrhofer. [28] However, since it is difficult to track and keep count of the volume and dimensions of the carbon support, we cannot completely rule out the fact that the lost in particle count is due to the coalescence of particles.

44

TABLE 5-1 AVERAGE PARTICLE DIAMETER OF PT-FE (PRIOR AND AFTER ELECTROCHEMICAL CYCLING)

Sample	Average Diameter
Pt3Fe - Prior Cycling	4.24 nm
Pt3Fe - After Cycling	5.13 nm
Pt3Fe2- Prior Cycling	3.18 nm
Pt3Fe2- After Cycling	4.19 nm

Detailed inspection of HRTEM images show that Pt-Fe particles commonly exhibit facets with low index planes including (001), (111), and (110). Conversely, high index planes produce greater surface defects including steps and kinks, which are excellent active sites. However, these surfaces also have high surface energy, which makes them unstable and difficult to form. Wang et. al. [40] investigated the morphology of platinum bimetallic alloys and concluded that platinum alloys generally form cuboctahedral shapes as a result of low index planes termination.[41–44] Nanoparticles tend to facet in order to increase the number of low index planes to decrease their surface energy. In terms of growth mechanism, the formation of the cuboctahedral structure results from the combination of triangular and octagonal nuclei on the {110} and {111} facets, respectively. However this trend is not observable in the Pt-Fe particles as their shapes appear irregular with some elongated asymmetrical structures. Irregularly shaped low index facets and particle size variation observed from the Pt-Fe nanoparticles can be traced back to the synthesis process. The control of degree of supersaturation in colloidal synthesis plays a key role for the particle size distribution. During particle synthesis, there must be a clear separation between

45

nucleation and growth to obtain a uniform size.[45] Furthermore, the irregularly-shaped nanoparticles are associated with the number of twin defects in the seed crystals and subsequent fast reaction growth. Therefore, the unique morphology of the Pt-Fe particles, suggests irregularly-shaped, fast reacting nuclei that grow into asymmetrical particles.[46–48]

5.1.2. HIGH ANGLE ANNULAR DARK FIELD IMAGING

High angle annular dark field imaging was performed on the Pt-Fe nanoparticles. In the case for Pt and Fe, platinum atoms (Z = 78) would produce a much brighter contrast than iron atoms (Z = 26). As a consequence, this technique is also extremely powerful in determining the ordering of the atoms when the particle is along its zone axis.[49]
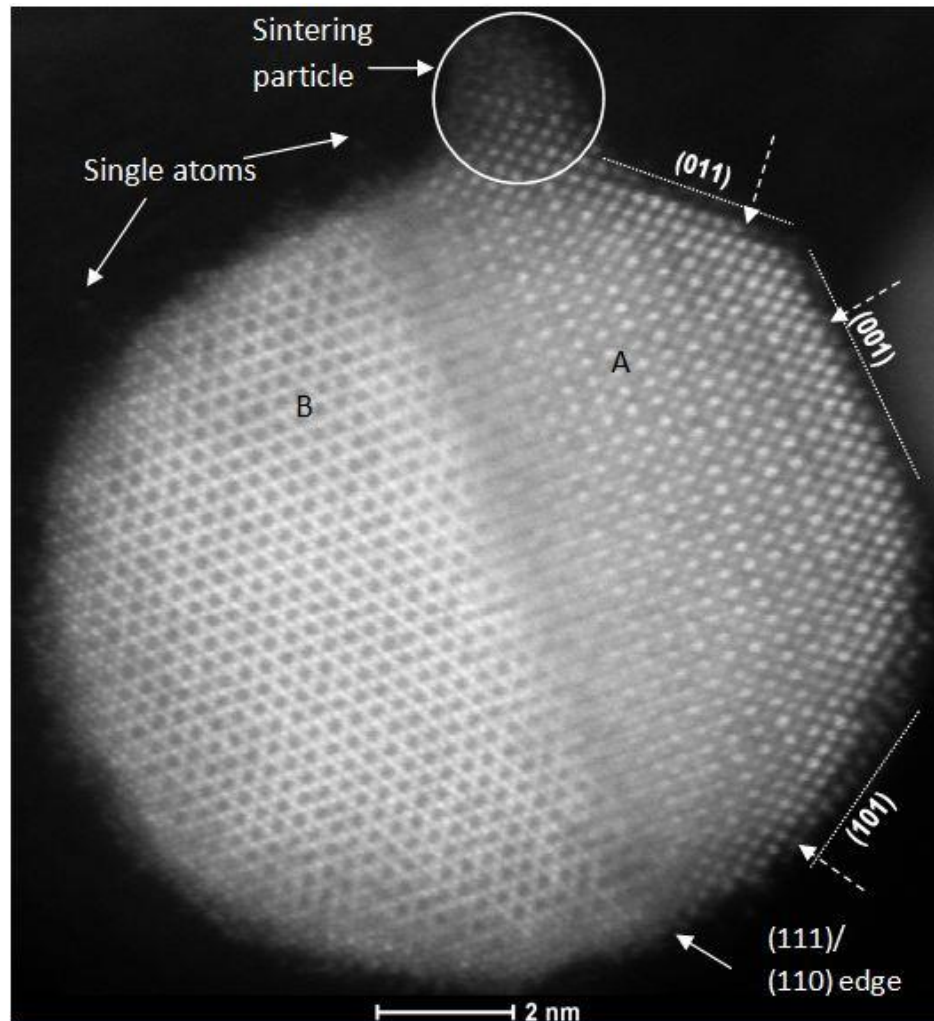
FIGURE 5-4 12NM PT-FE NANOPARTICLE SHOWING A NUMBER OF FEATURES INCLUDING ORDERING, FACETS, AND MONOATOMIC STEPS

We now focus on the detailed analysis of the crystallography and surfaces of particles to understand their structure. Figure 5-4 shows an HAADF image of a 12 nm Pt_3Fe particle exhibiting two different crystal orientations possibly arising from two particles merging during synthesis at high temperature. This particle is highly ordered with the left and right half portions of the particle oriented along [111] and [110] zone axes, respectively. There is a clear boundary that separates the two sub- nanocrystals

near the center of the particle. The periodic pattern with alternating bright columns and dark columns in the HAADF image, particularly in the central part of the two distinct regions (indicated by the labels A and B) in Figure 5-4, suggests that there is a sublattice with Pt-Fe ordering. To further confirm the ordering of this particle, an HAADF simulation of the ordered and disordered Pt_3Fe crystal structure of the particle is presented in Figure 5-5 a to d. Note that the iron columns are not detected in the [111] orientation due to the dominating contrast produced by the six platinum columns surrounding the Fe column in a hexagonal pattern. It is also obvious that the [110] orientation produces atomic columns with alternating intensities. The brighter columns are the platinum-only columns, whereas the darker columns originate from both platinum and iron atoms on the same column in the direction of the electron beam (Figure 5-5 g). Simulations using a fully disordered Pt_3Fe structure (Figure 5-5 b and d) with Pt and Fe atoms distributed randomly on the same lattice sites show no particular repetitive pattern with high and low intensities. By comparing the atomically resolved HAADF images with the simulations, it is evident that the Pt_3Fe phase in the nanoparticles is highly ordered. Figure 5-5 e) and f) illustrates the projection of the unit cell along the [111] and [110] orientation thus demonstrating the model structure used in the simulations.
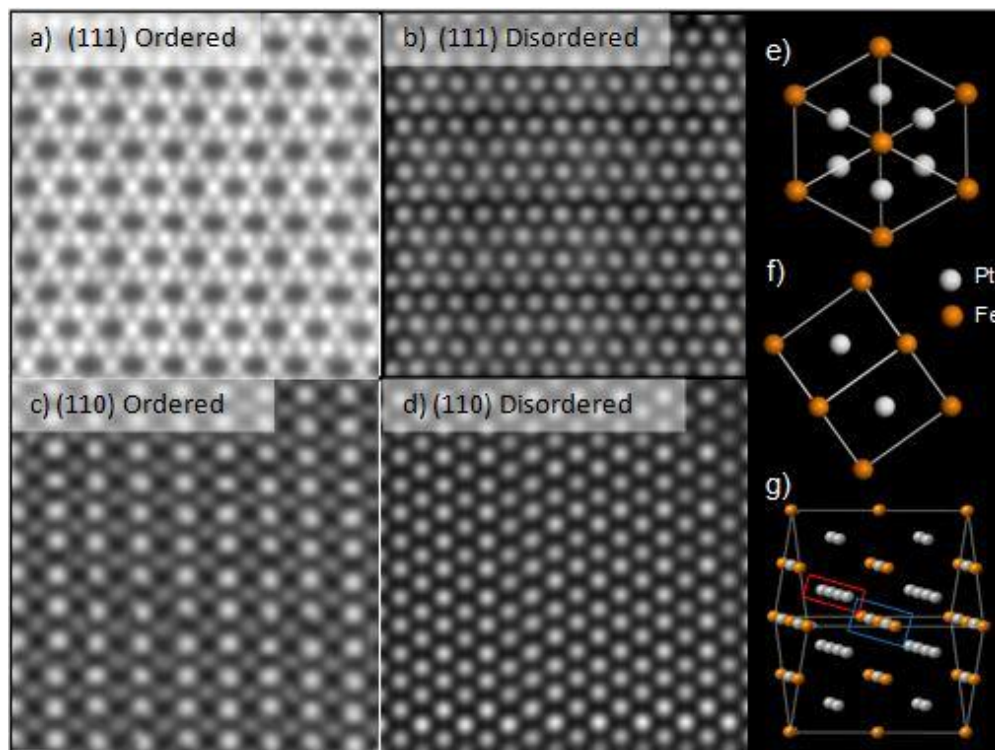
FIGURE 5-5 A -D SIMULATIONS OF ORDERED AND DISORDERED STRUCTURES; E –F PROJECTION OF 111 AND 110 ZONE AXIS RESPECTIVELY; G DIFFERENCE OF PT RICH AND FE RICH COLUMNS

Aside from the difference in crystal orientations, a number of remarkable features can be identified from this nanoparticle. As indicated by the dashed arrows in Figure 5-4, there are a number of mono-atomic steps and islands forming at the surface of the particle. In addition, from the [110] projection it is obvious that faceting on (011), (001), and (010) planes on the surface are present. These observations of steps and facets are highly significant as these are likely reactive sites for the adsorption of hydrogen or oxygen.[50] There are also single Pt atoms (based on the intensity as compared to the carbon background) on the carbon- support in the vicinity of the particle, possibly diffusing to the large crystal from neighboring particles or residues

49

from dissolution of the large particles. Lastly, the small extrusion near the top of the

12nm particle is strong evidence of the coalescence of a small particle with the large one.

It is interesting to point out that the orientation of the smaller particle is perfectly

aligned with the large one following rotation of the lattice during the coalescence.
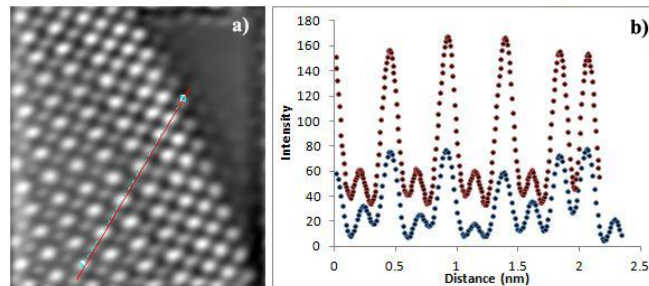
FIGURE 5-6 A) FFT FILTERED HAADF IMAGE OF PT-FE NANOPARTICLES; B) INTENSITY PROFILES
FROM THE LINE SCAN OF A AND SIMULATION ASSUMING A PT RICH OUTER SHELL TWO ATOMIC
LAYERS THICK

Detailed inspection of the surface of the particle in Figure 5-4 also reveals a

change in the ordering in the outer layers of the nanoparticles area in the [110]

orientation. Due to the fact that the contrast between the Pt and Fe columns of HAADF

images is monotonic with the sample's thickness, this observation in Figure 5-6 suggests

that iron ordering starts 2 to 3 atomic layers below the nanoparticles' surface, hence

giving evidence for a platinum rich surface.[40] These observations are significant in

terms of catalytic activity. First of all, a core-shell structure having a platinum rich

surface is expected to be highly beneficial due to the optimization of platinum usage

and active surface sites. Secondly, several reports have proposed that a thin Pt enriched

or Pt only surface layer on top of an alloy structure enhances the ORR activity.[12] Given

the importance of this observation and in order to further validate this observation for

the Pt-Fe particles more quantitatively, the HAADF intensity profile of ten atomic layers below surface of the particle is compared with a core shell simulated particle presented in Figure 5-6. The well-defined Pt shell is confirmed by the higher intensity peaks produced by the outer surface of the particle. The simulated particle that exhibits this same contrast would thus exhibit a platinum rich surface of over two atomic layers in which the intensity profile is comparable to the experimental HAADF image intensity profile.

Figure 5-7 shows another example of an atomically resolved image of a large Pt-Fe nanoparticle. Figure 5-7 is a 12 nm Pt_3Fe_2 nanoparticle. Similar to Figure 5-4, this is a bi-crystal with the right side oriented in the (110) zone axis. The orientation on the left side of the particle is undetermined due to the fact that its tilted out of axis. Again, there is a high degree of ordering, as determined by the alternating rows of platinum-rich and iron-rich columns (alternating rows of bright and dark columns). As indicated by the circles, the surface of the particle contains only similar high intensity columns which is suggesting a platinum rich surface. Furthermore, the unique shape of this particle is possibily created by the coalence and merging of two smaller crystals, resulting in the boundary observed in the middle, as well as the kinks on the bottom and top where the two individual crystals meet. The round edges and surface make up the monoatomic steps, as well as atomic terrance, which acts as adsorption sites for catalytic reactions as indicated by the arrows.
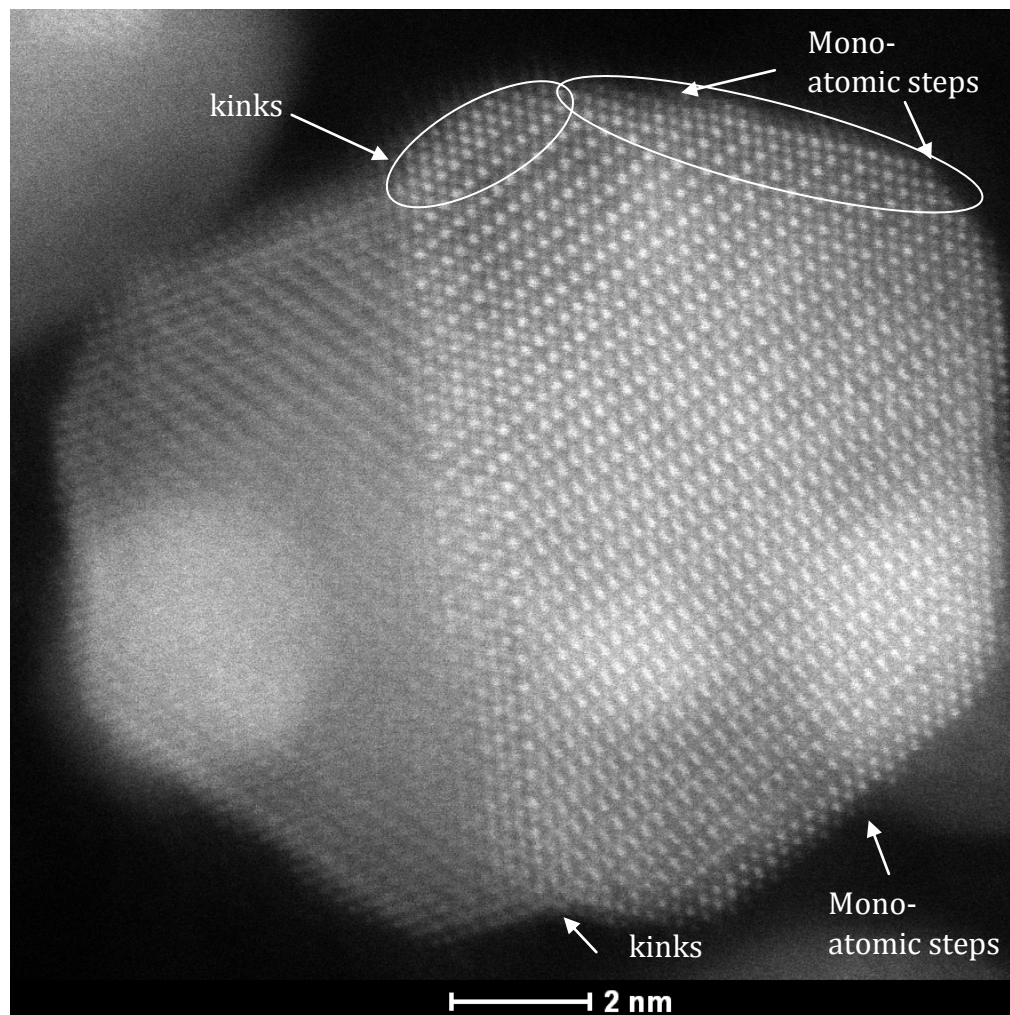
FIGURE 5-7 ATOMICALLY RESOLVED PT3FE2 PARTICLE SHOWING HIGH DEGREE OF ORDERING

Ordering of Pt and Fe in atomic columns was also observed for small nanoparticles in the size range of 2 to 4 nm, but unlike the larger particles, the majority of the smaller particles tend to be single crystals as shown in Figure 5-8 a and b. Figure 5-8 c shows a 4 nm diameter particle ordered in the 001 orientation for one half of the particle and the other half tilted out of the zone axis. Similar to the larger particles, surface steps, and truncated corners are therefore also observed.

It is well known that the surfaces of Pt (100), (111), and (110) are all stable sites for oxygen; specifically, the (111) surface is the most active and stable.[15] Different facets yielding different activities can be explained by the variance of surface energies and energy bands associated with different planes. In general, the (111) plane has the lowest surface energy followed by (100) then (110).[14] Gu et. al. [15] performed density functional theory calculations on oxygen absorption on platinum surfaces. On the surface of the platinum, there are a number of different adsorption sites that oxygen is favorable to. Aside from the surfaces, it is possible for oxygen atoms to be absorbed inside the subsurface within one monolayer below the surface.[16] All of these low index planes and active sites are observed in the Pt-Fe particles, which indicate that Pt-Fe as an excellent candidate to be used for the ORR. This indeed is confirmed by the high specific ORR activities measured for these catalysts.[51]

5.1.3. ELEMENTAL ANALYSIS

Energy dispersive X-ray spectrometry (EDXS) was performed on the Pt-Fe samples to extract the compositional information of the nanoparticles. Performing EDXS allows us to obtain localized information regarding the composition of the sample . For example, various EDXS techniques including line scan, area scans, and mapping to correlate the atomic composition with the atomic coordinates. Especially for unique catalyst designs such as a core shell structure, EDXS is an unavoidable tool in the design verification process.

Individual nanoparticles with different sizes were scanned using EDXS to determine the compositional influence of electrochemical cycling (E-cycling). The summary of the Pt and Fe atomic concentration of individual particles plotted as a function of particle size obtained from EDXS measurements is shown in Figure 5-9. A dependency of the Fe composition on the particle size is observed for both of the as-prepared samples. Larger particles have a higher Fe content that is essentially the same as the corresponding nominal ratio (75:25 and 60:40 for Pt_3Fe and Pt_3Fe_2 respectively). In the case of the small (as-prepared) particles, the Fe content is less than the nominal ratios and this is consistent for both of our samples. Referring to Figure 5-9, a significant decrease in Fe concentration can be observed after electrochemical cycling for both samples. This drop in iron content is part of the catalyst degradation process which is undesirable. Based on this EDXS information, it confirms that the iron is dealloyed from the nanoparticle during the cycling process. Referring to Figure 5-9, it is observed that

54

the Pt$_3$Fe sample has a greater loss of iron after cycling with no correlations to the particle size, as the majority of the iron decreased to approximately 10%. On the other hand, larger particles (diameter > 10nm) of Pt$_3$Fe$_2$ contain higher iron content as shown in Figure 5-9. This discrepancy could possibly be due to the greater initial iron content for Pt$_3$Fe$_2$. However a greater sampling size is required in order to verify this trend.
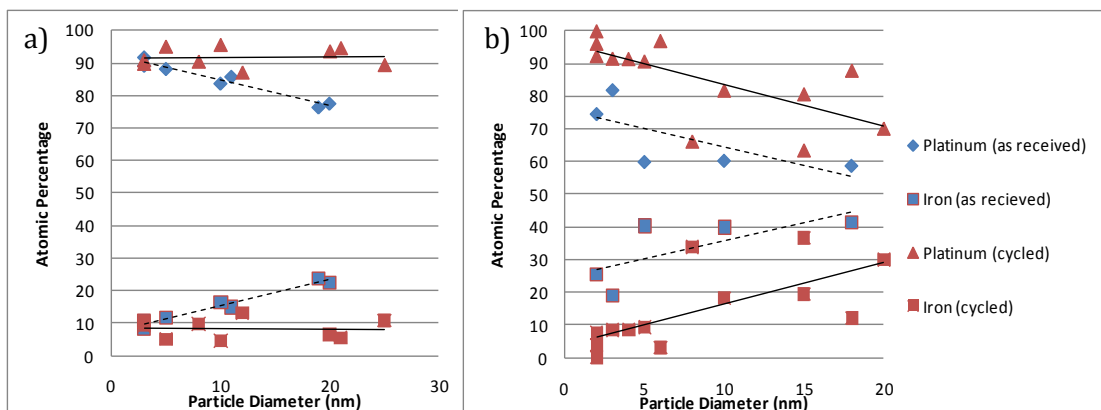
FIGURE 5-9 EDX SCAN ON INDIVIDUAL PARTICLES CORRELATING ATOMIC PERCENTAGE WITH PARTICLE SIZE; A) AND B) SHOW RESULTS FOR PT3FE AND PT3FE2 RESPECTIVELY PRIOR AND AFTER ELECTROCHEMICAL CYCLING

EDXS line scans were employed to investigate the elemental distribution across the catalyst particles after 10,000 cycles. Figure 5-10 a shows the example of a 19 nm Pt$_3$Fe particle. The blue line indicates the atomic percentage of Pt and Fe before cycling. As presented, the atomic distribution is evenly distributed across the particle with a Pt:Fe ratio of 75:25. The red line shows the atomic ratio after electrochemical cycling. As we can see, potential cycling caused significant changes in composition. Specifically, cycling resulted in higher iron content in the center of the particle and a higher platinum content on the side, thus suggesting a core shell structure caused by electrochemical

treatment. The results here agree with the work performed by Chen et al[24]. However, this core shell structure is not always observable as shown in Figure 5-10 b. Figure 5-10 b illustrates a similar sized particle, but with iron segregating to one side of the particle after electrochemical cycling. Therefore, it would be more appropriate to suggest that electrochemical cycling causes phase segregation and significant changes in atomic composition. It should be mentioned that the particles before and after electrochemically cycling are different particles having the same size. However, the EDXS line scans are conclusive since the line scans before cycling is always evenly distributed whereas the cycled particles are always segregated.
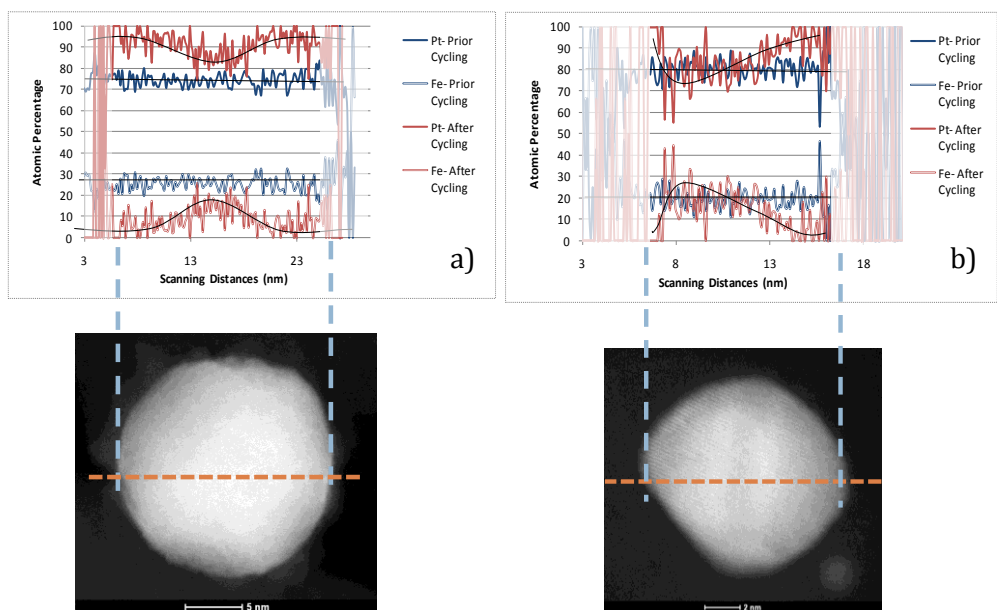
FIGURE 5-10 EDX LINE SCAN CORRELATING THE ATOMIC PERCENTAGE WITH ATOMIC COORDINATES BEFORE AND AFTER ELECTROEHCMICAL CYCLING

In order to further investigate the structure of the catalysts after 10,000 cycles, EDXS local measurements were carried out at the edges and the center of the particles

for comparison. Figure 5-11 shows the example of this analysis for a 15 nm sized catalyst

particle for both before and after cycling. Prior to cycling, the platinum atomic

concentration is the same (approximately 58%) at three different locations as shown in

Figure 5-11 a. After cycling, the atomic concentrations of Pt to Pt+Fe are determined as

68.8 (left edge), 89.9 (right edge) and 57.8 (center position) %. This supplements the

evidence that phase separation can be caused by electrochemical cycling. Since the

particles are extremely small and the absorption can be neglected, these results suggest

that the surface of the large Pt_3Fe_2 catalyst particle consists of two "phases", a Pt-

enriched shell and a Pt+Fe core.
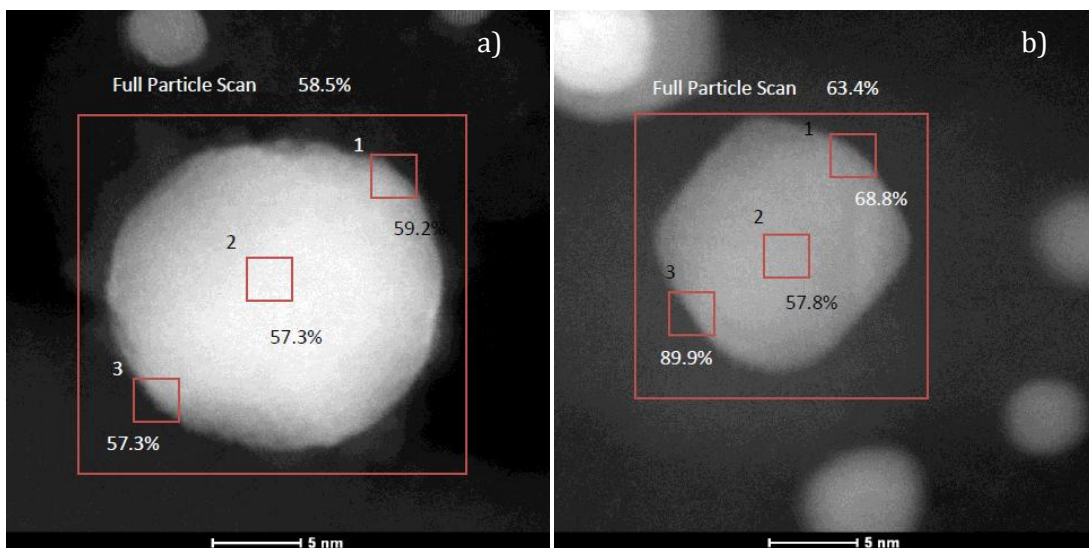
FIGURE 5-11 EDX LOCAL MEASUREMENTS DETERMINING ATOMIC PERCENTAGE AT VARIOUS LOCATIONS; NUMBERS SHOWN BESIDE BOX INDICATE LOCAL PT ATOMIC PERCENTAGE. A) AND B) SHOWS RESULTS BEFORE AND AFTER ELECTROEHCMIAL CYCLING RESPECTIVELY

The core shell structure is further confirmed by EDXS mapping of Pt and Fe after

electrochemical cycling shown in Figure 5-12. The EDXS mapping results are obtained

with much more efficient detectors that have about 10 times the collecting efficiency

than regular detectors, where the potential beam-induced loss can be excluded during

the very short acquisition time. Referring to Figure 5-12, the green map shows the

location of the platinum, whereas the red map shows the location of iron. With the two

colour maps combined, the relative position of each element is revealed. Larger

particles show a concentrated red core (iron) while having a ring of green on the edge

indicating a core shell structure. However, as indicated by the dashed arrows, selective

small particles have small portions of iron segregating to one side and some particles

(solid arrows) are seen to mainly consist of Pt (green) only. The above results suggest

that the formation of core shell structure is dependent on the particle size. For example,

platinum rich particles are only observed for particles less than 5nm, and defined core

shell structures are only observed for particles greater than 10nm. If there is a better

control of particle size, it might be possible to have better control in the core shell

structure.
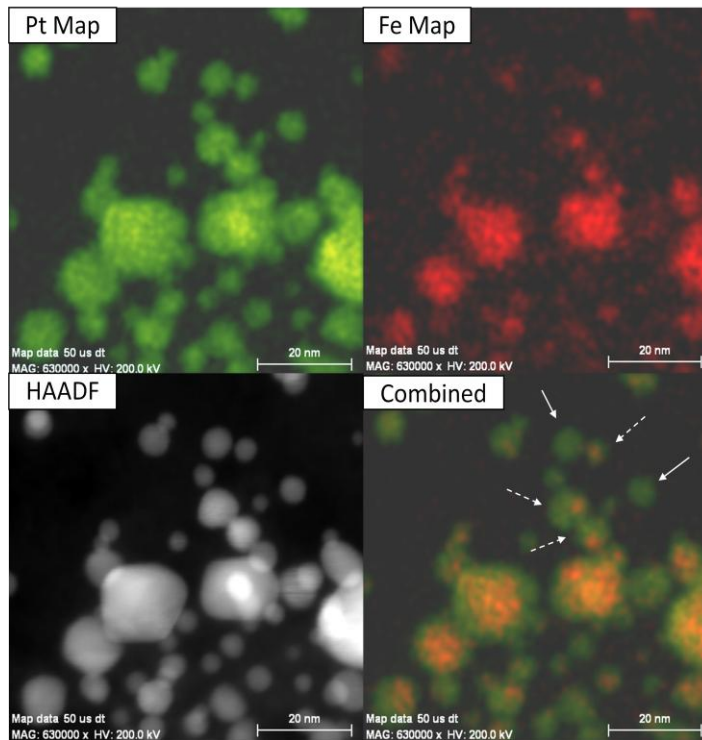
FIGURE 5-12 EDX MAPPING SHOWING RELATIVE LOCATION OF PT AND FE

In summary, EDXS provides strong evidence that the phase separation occurs after E-cycling and the results are consistent for the various EDXS methods used. Prior to potential cycling, the atomic concentrations are always evenly distributed across the particle. Once the particles are cycled 10,000 times, phase segregation occurs with lowered iron concentration (more evident for particles less than 5nm). In certain cases, particularly for larger particles, (>10nm in diameter) core shell structures are formed having an iron + platinum core and platinum shell. For smaller particles, iron segregation occurs and thus some particles are composed of platinum only.

5.1.4. ATOMIC DISPLACEMENT CALCULATIONS

Surface atoms have a lower coordination than bulk atoms, therefore, surface relaxation is expected to occur.[14] This would result to a change of the interlayer distance at the surface compared to the core of the particle. The measurement of surface relaxation is possible with the atomically resolved HAADF image shown in Figure 5-13. Prior to the calculation, the image is FFT filtered to reduce the noise. The local positions of the maxima of each atomic column are determined by a 2D Gaussian function within Matlab scripts to locate the column centers as shown by the green crosses in Figure 5-13 a. Lastly, the local maxima at the center of the particle are used as a reference to extrapolate the locations of the atoms as shown by the red crosses. Knowing the local maxima allows the determination of the (001) inter-atomic distances. The first two atomic layers are the areas of interest as they are the locations of active sites. Consistent with previous studies,[52] surface relaxation results in larger atomic displacements in the outer layers of the particle with the average displacement of 19.6 pm. As shown in Figure 5-13 b, the displacement magnitude varies from atom to atom though the majority of the atoms are displaced by roughly 10 pm. The majority of the atoms in the outer-most layers expanded outwards, whereas a few atomic columns compressed inwards. Selective columns displaced over 60 pm in the outer first and second atomic layers. Du et. al. [52] performed a study on platinum interatomic distances and suggested the large expansion in the outer layer is possibly due to the formation of Pt-O-Pt bonds in which the oxygen cannot be observed.[52] The presence

of the induced strain, steps, and islands is likely one of the key factors that affect the

catalytic activity.[12]
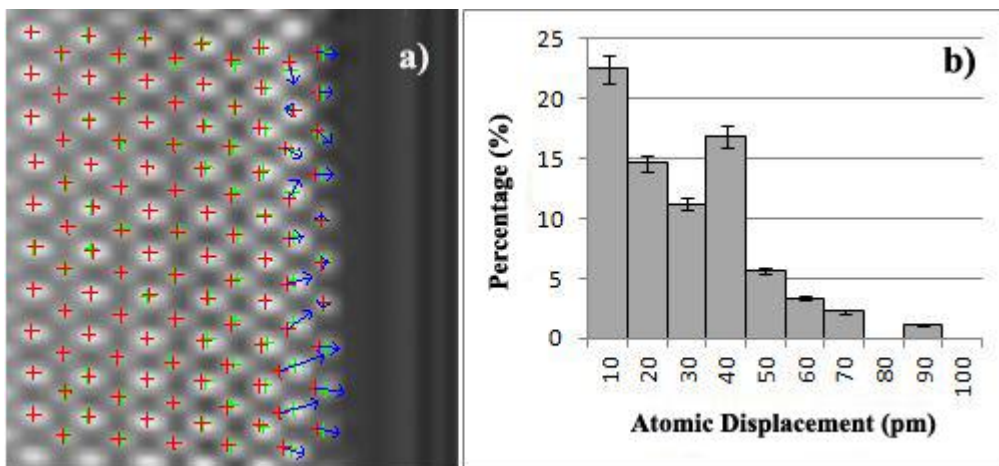
FIGURE 5-13 ATOMIC DISPLACEMENT CALCULATIONS OF (110) PT3FE PARTICLE SURFACE. GREEN AND RED CROSSES ARE THE ATOMIC LOCAL MAXIMUM AND THE EXTRAPOLATED REFERENCES RESPECTIVELY. ARROWS ARE VECTORS THAT SHOW THE DIRECTION AND MAGNITUDE OF DISPLACEMENTS

5.1.5. DETERMINING UNKNOWN CRYSTAL STRUCTURE

Pt_3Fe compound exists in the bulk phase and is a common and widely studied

phase with a known crystal structure type of cubic $L1_2$ Au-Cu. On the other hand, Pt_3Fe_2

is an uncommon composition. Based on the highly ordered nanoparticles of Pt_3Fe_2

obtained from HAADF imaging, attempts were made to solve the unknown crystal

structure of Pt_3Fe_2. Sanati et. al.[16] Investigated the crystal structure type of Au-Cu and

proposed that Au_3Cu_2 is a superstructure containing 12 Au and 8 Cu atoms. Using the

same model by Sanati, the superstructure of Pt_3Fe_2 is proposed as shown in Figure 5-14.
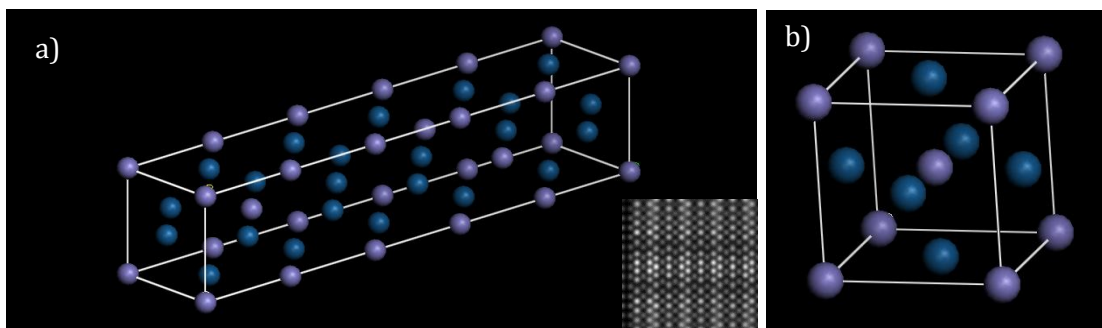
FIGURE 5-14 HYPOTHESIZED STRUCTURES OF PT3FE2. A- SUPERSTRUCTURE CONTAINING 12 PT AND 8 FE; B- PTFE3 CUBIC CRYSTAL WITH ADDITIONAL FE ATOM IN CENTER

However, the multi-slice simulations of the suggested superstructure do not match with the experimental ordering shown in the HAADF as shown in the inset of Figure 5-14 a. Another possible unit cell with a 3:2 Pt:Fe ratio would be simply placing an iron atom in the center of the cubic unit cell as displayed in Figure 5-14 b. Nevertheless the (110) projection of such structure would not result in the repeating pattern as observed in Figure 5-7 which eliminates this model. Comparing the HAADF images of the two catalysts, it is evident that the Pt-Fe order of the two compositions is very similar since the patterns for the same orientation appear to be very similar, at least qualitatively. EDXS results of the particle cluster gives a Pt:Fe atomic ratio of 77:23 ± 7 % and 64:36 ± 5 % for Pt_3Fe and Pt_3Fe_2,respectively. This confirms that there is a quantitative difference in atomic composition of the two types of samples, thus suggesting different unit cell structures. More specifically, the atomic composition of individual particles was obtained using EDXS spot analysis as presented in Figure 5-15. It is clearly shown that individual particles larger than 5nm have a consistent Pt:Fe ratio of approximately 60:40 which matched with the nominal ratio. However, smaller particles in the size of 2 to 3

nm exhibit up to 80% higher Pt content. Inspection of the bulk Pt-Fe phase diagram shows that alloys with the 60:40 composition are expected to be at the boundary between the $L1_0$ (PtFe) and $L1_2$ (Pt_3Fe) phases.[53]   However, individual particle elemental analysis gives no evidence of the $L1_0$ phase, thus strongly suggesting that that the $L1_0$ is not an appropriate structure for the Pt_3Fe_2 nanoparticles.
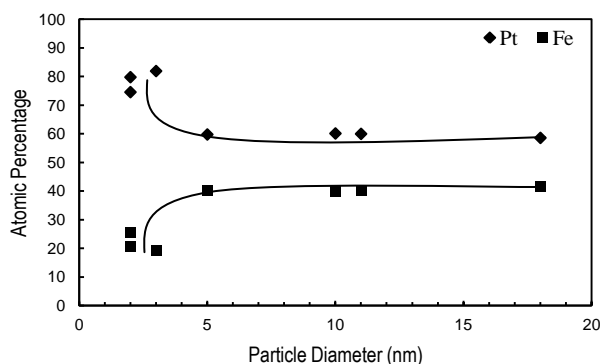
FIGURE 5-15 ATOMIC COMPOSITION VS PARTICLE SIZE FOR INDIVIDUAL PT3FE2 NANOPARTICLES

It is extremely difficult to determine the exact crystal structure of unique structures especially in the nano scale. As reported by Billinge et. al., a combination of different experimental methods as well as the use of simulations are required to solve a crystal structure. [54] To obtain complementary information regarding the crystal structure of the nanoparticles, X-ray powder diffractometry was performed for both systems. Diffraction patterns from crystalline materials present slightly broad peaks (Figure 5-16) from which it is possible to determine the interatomic spacing. The diffraction patterns of the two catalysts are qualitatively similar. However, detailed inspection of the diffraction pattern shows a splitting of the (220) and (002) reflections

for Pt_3Fe_2. Peak splitting to a higher 2θ value corresponds to the compression in the c

lattice from Pt_3Fe to Pt_3Fe_2, hence the change from cubic to tetragonal structure.
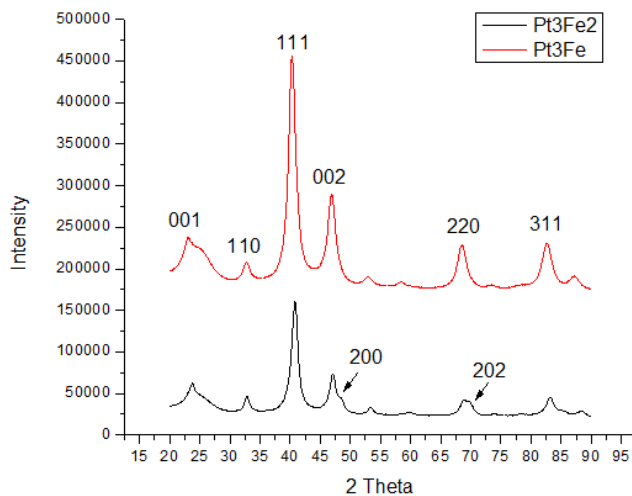
FIGURE 5-16 X-RAY DIFFRACTION PATTERN OF PT3FE (TOP) AND PT3FE2 (BOTTOM) NANOPARTICLES

Combing the XRD data with the TEM images and simulations, two different

Pt_3Fe_2 models are hypothesized: a single, partially ordered tetragonal phase and a

binary mixture of Pt_3Fe /PtFe phases. Based on the structure refinement with the X-ray

data, a single phase Pt_3Fe_2 model is possible with a partially ordered unit cell. The

deduced Pt_3Fe_2 would be a P4/mmm tetragonal structure having lattice parameters a,

and c of 3.865(4) and 3.769(3) respectively. The atomic coordinates of the hypothesized

model are listed in Table 5-2 with the proposed structure illustrated in Figure 5-17.

TABLE 5-2 ATOMIC COORDINATES FOR SUGGESTED SINGLE PHASE PT3FE2

X	Y	Z	Occupancy
0	0	0	1 Fe
0.5	0	0.5	1 Pt

0	0.5	0.5	1 Pt
0.5	0.5	0	0.4 Pt/ 0.6 Fe

Referring to Figure 5-17, the orange and white atoms are iron and platinum respectively whereas the green atoms are the randomly ordered atoms with 40% platinum and 60% iron. The placement of the iron atoms in the edge of the tetragonal unit cell would retain the ordering as shown in the [110] and [001] orientations in agreement with the ordering observed in HAADF. In comparison, the difference in the Pt:Fe compositional ratio from Pt_3Fe would only arise from the randomly ordered layer along the c/2 plane on the unit cell. This proposed model would yield an overall atomic ratio of 60:40 % in agreement with the EDXS results. It should be mentioned that a number of different single phase partially ordered models were tested and the reported structure gives the best refinement RWP value of 5.995.
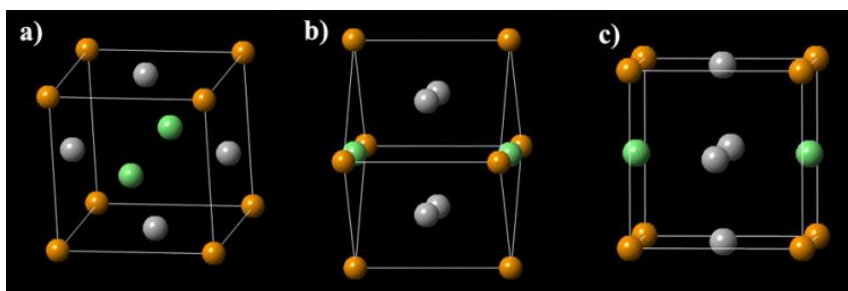
FIGURE 5-17 A- SUGGESTED SINGLE PHASE PARTIALLY ORDERED PT3FE2 TETRAGONAL UNIT CELL. ORANGE AND WHITE ATOMS ARE IRON AND PLATINUM RESPECTIVELY. THE 2 GREEN ATOMS ARE THE RANDOMLY ORDERED ATOMS BEING 40% PT AND 60% FE; B AND C ARE THE 110 AND 110 ORIENTATIONS

The second suggested model of Pt_3Fe_2 consists of the two known Pt_3Fe and PtFe phases. This mixed phase model is a combination of the cubic Pm-3m and the tetragonal P4/mmm crystals. The XRD structure refinement yields a RWP value of 3.8 and a

compositional atomic of 49.27% and 50.73% Pt_3Fe and PtFe, respectively. As mentioned earlier, individual nanoparticle EDX analysis shows no evidence of a PtFt phase, however due to the lower RWP value produced in the refinement, the mixed phase model remains to be a possible atomic structure for Pt_3Fe_2. The bulk powder used for the X-ray measurement may contain a significant amount of very small nanoparticles, with a Pt-Fe phase variation as shown in Figure 5-15.

5.1.6. ELECTROCHEMICAL PERFORMANCES

The selection of fuel cell catalyst comes down to the electrochemical performance of the material. The electrochemical measurements of catalysts is often done by performing cyclic voltammetry (CV) since it is a simple tool for assessing the durability of the catalysts outside of an actual fuel cell. For fuel cell applications, the reaction of interest is the oxygen reduction reaction (ORR) at the cathode as that is the rate limiting step for the overall system. The ORR activity can be obtained from a CV curve and is generally quantified by measuring the current at 0.9V (vs RHE) and dividing this current by the platinum mass or the surface area to get the mass and specific activity respectively. It is important to note that both the mass and the specific activities should be considered since the mass activity dictates the platinum loading whereas the specific activity is a more fundamental measurement of the intrinsic activity of the material. [55]
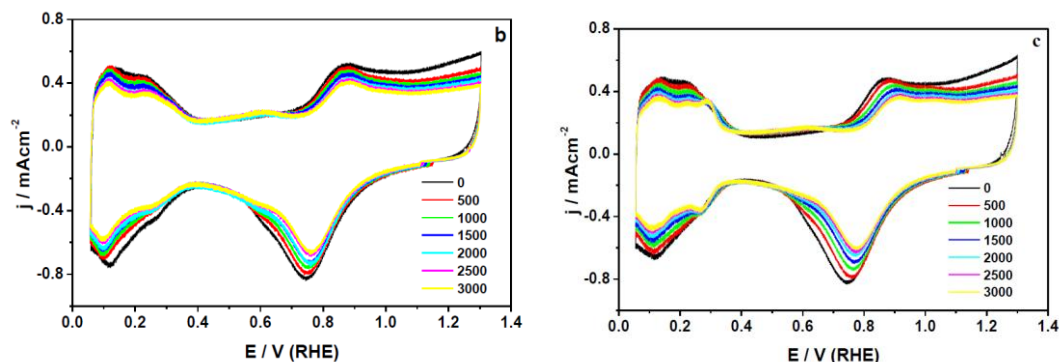
FIGURE 5-5-18 CYCLIC VOLTAMMOGRAM OF PT3FE (LEFT) AND PT3FE2 (RIGHT) OVER THE
COURSE OF 3000 ELECTROCHEMICAL CYCLES

Figure 5-5-18 above shows a CV curve of Pt_3Fe and Pt_3Fe_2 taken over the course of 3000

E-cycles between 0 to 1.3V with a sweep rate of 50 mV s^{-1}. The different colour lines

show the number of cyclings starting at zero with increments of 500. Both CVs produced

a similar trend. Focusing at the hydrogen adsorption and desorption peaks (0 – 0.4V vs.

RHE), we see that the current deceases as cycling increases. This indicates a decrease in

electrochemical surface area (ECSA) during the cycling process. The drop in surface area

is most likely due to nanoparticles dissolution, agglomeration, and falling off the

support. Looking at the cathodic current at 0.9V, it is evident that activity decreases with

extensive cycling. Quantitatively, the mass activity dropped from 0.22 to 0.11 A mg^{-1} and

the specific activity dropped from 509 to 473 μAcm^{-2} for Pt_3Fe. On the other hand,

Pt_3Fe_2 produced a mass activity of 0.23 and 0.11 A mg^{-1} before and after cycling

respectively and a specific activity of 550 and 496 μAcm^{-2} before and after cycling

correspondingly. It is worthy to mention that both of these Pt-Fe alloys produced a

much higher catalytic activity compared to pure platinum (Pt having a mass and specific

67

activity of 0.07 A mg^{-1} and 215 µAcm^{-2} respectively) Overall it is clear that electrochemical cycling causes a decrease in activity which is part of the degradation of the catalyst.

Although the current bimetallic alloy produces an enhanced activity that is three times higher than pure platinum, the target activity is still unachieved. As stated in the Fuel Cell Technical Plan by the US Department of Energy, the target mass activity for the year 2017 is 0.44 A/mg compared to the current status of 0.23 A/mg. Therefore, futhre work must be placed in terms of the design of the catalysts and fine turning of the active sites. [56]

5.1.7. SUMMARY OF PT-FE CATALYTIC NANOPARTICLES

Two different Pt-Fe compositions were characterized by transmission electron microscopy including Pt_3Fe_2 and Pt_3Fe. Both compositions show a wide size distribution from approximately 1 to 25 nm in diameter with a mode and median at $2 - 3$ nm. The particles appear to be sphere-like in shape with a number of truncated edges. High angle annular dark field images show atomically resolved structures with high degrees of ordering. In addition, a number of low indexed facets and defects (including surface steps, atomic displacements, and surface edges) were identified which makes these Pt-Fe nanoparticles an excellent candidate for catalysis applications. Electrochemically cycling the catalysts 10,000 times caused an increase in particle size as well as atomic phase separation. It is evident that selective particles formed a platinum rich surface

after the electrochemical treatment. Lastly, two different models of Pt_3Fe_2 phase are suggested by combining data from HAADF and XRD.

5.2. PT-CO CATALYSTS

Pt-Co is another candidate for fuel cell catalysts. Similar to Pt-Fe, the addition of cobalt results in the change in lattice parameter that leads to higher catalytic activity. In theory, referring to the volcanic diagram in Figure 2-1, Pt-Co particles would produce a higher activity compared to Pt-Fe due to the faster dissociation rate of oxygen with the use of the cobalt alloy. Specifically, the Pt-Co catalysts were used to study the degradation of the catalyst on high surface area carbon support as the samples were potentially cycled at low and high cycles (60 and 3000 times respectively).

5.2.1. THE EFFECT OF ELECTROCHEMICAL CYCLING ON PARTICLE MORPHOLOGY

Recall that one of the objectives is to study the electrochemical cycling effect on the morphology and the composition of the nanoparticles. In practical fuel cell usage, potentials are being applied onto the catalysts hence electrochemical cycling is part of the catalyst degradation study. As part of the industrial standards, it is desirable to have a fuel cell life time of greater than 5000 hours.

The following TEM results show the effect of electrochemical treatment on high surface area carbon supported Pt-Co nanoparticles. Three different sets of samples (as

synthesized, 60 cycles, and 3000 cycles) were characterized. Information regarding particle size, shape, and composition were compared to determine to effect of electrochemical cycling. Figure 5-19 below shows the general particle shape and morphology of as synthesized, 60 cycles, and 3000 cycles Pt-Co nanoparticles respectively. The cloud-like shaped structures are the Ketjen carbon support with high surface area. The majority of the particles have a sphere- like shape with some irregular elongated truncated structures. Comparing the as synthesized with the 60 cycles nanoparticles, no major differences are observed (Figure 5-19 a and b). Both samples show evenly and densely distributed Pt-Co nanoparticles on the carbon support. However, the samples that were cycled 6000 times (Figure 5-19 c) shows two remarkable changes in the morphology. Firstly, there is a significant increase in particle size which is qualitatively observable. Secondly, there is a reduction in particles on the supporting material as the carbon supports are much less populated. Similar to the Pt-Fe nanoparticles, the increase in particle size after cycling is attributed to Oswald ripening and coalescence. For the samples that were cycled 3000 times, enough energy was supplied into the catalyst such that smaller particles would prefer to migrate into larger particles to decrease surface energy. The diffusion process could happen by the diffusion of individual atoms, or by migrating and sintering with other particles. Both would result in the larger particles observed.
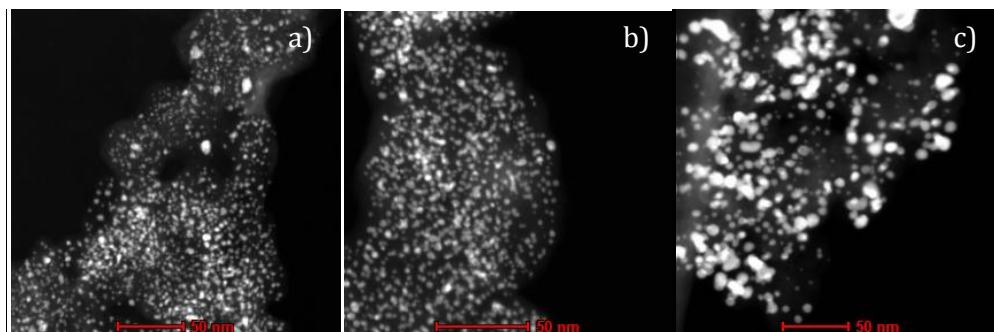
FIGURE 5-19 STEM DARK FIELD IMAGES OF PT-CO NANOPARTICES ON KETJEN BLACK SUPPORT. A. B, AND C SHOWS TYPICAL CLUSTERS FOR AS PREPARED, 60 CYCLES, AND 3000 CYCLES SAMPLES

Quantitatively, the particle size distribution is obtained by counting approximately the same number of particles from a series of images of each sample as illustrated in Figure 5-20. The average diameters are tabulated in Table 5-3. As expected, both the as synthesized and 60 cycles samples produced a similar average diameter of 2.7nm with a similar distribution of size ranging from approximately 1 to 5 nm. On the other hand, the particles that were cycled 3000 times have an increased average diameter of 4.4 nm with a much larger spread from 1 to 15 nm. Comparing the size distribution of Pt-Co to Pt-Fe in the previous section, we see that there is a much better control and a narrower spread in terms of particle size.
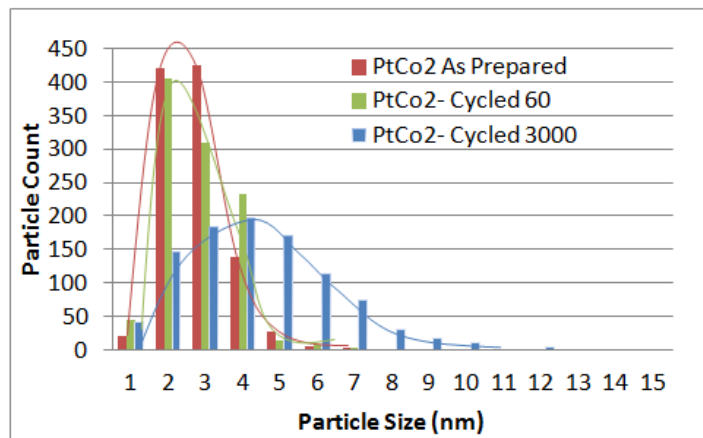
FIGURE 5-20 PARTICLE SIZE DISTRIBUTION OF PT-CO NANOPARTICLES

TABLE 5-3 AVERAGE PARTICLE DIAMETER FOR PT-CO NANOPARTICLES

Sample	Particles Counted	Average Diameter (nm)
PtCo2 As prepared	1038	2.76
PtCo2 Cycled 60	1016	2.77
PtCo2 Cycled 3000	1003	4.44

5.2.2. THE EFFECT OF ELECTROCHEMICAL CYCLING ON PARTICLE COMPOSITION

To obtain compositional information, energy dispersive X rays microanalysis was performed on individual nanoparticles to correlate the particle size with the platinum concentration as illustrated in Figure 5-21. The as-synthesized nanoparticles produced a Pt:Co ratio of roughly 60:40. Unlike the particle morphology, electrochemical cycling of the particles 60 times caused a significant change in the composition as the Pt:Co ratio changed to approximately 80:20. This change is consistent as a number of different

particles were scanned and none of them produced a Co concentration of over 20% after cycling 60 times. The samples that were cycled 3000 times produced an even lower average of Co concentration of approximately 10%. By studying all three plots in Figure 5-21, it is evident that all samples show a general trend towards a greater Pt content as the particle size increases. This is expected especially if the cycling produces a core shell structure with a greater Pt to Pt+Co ratio.
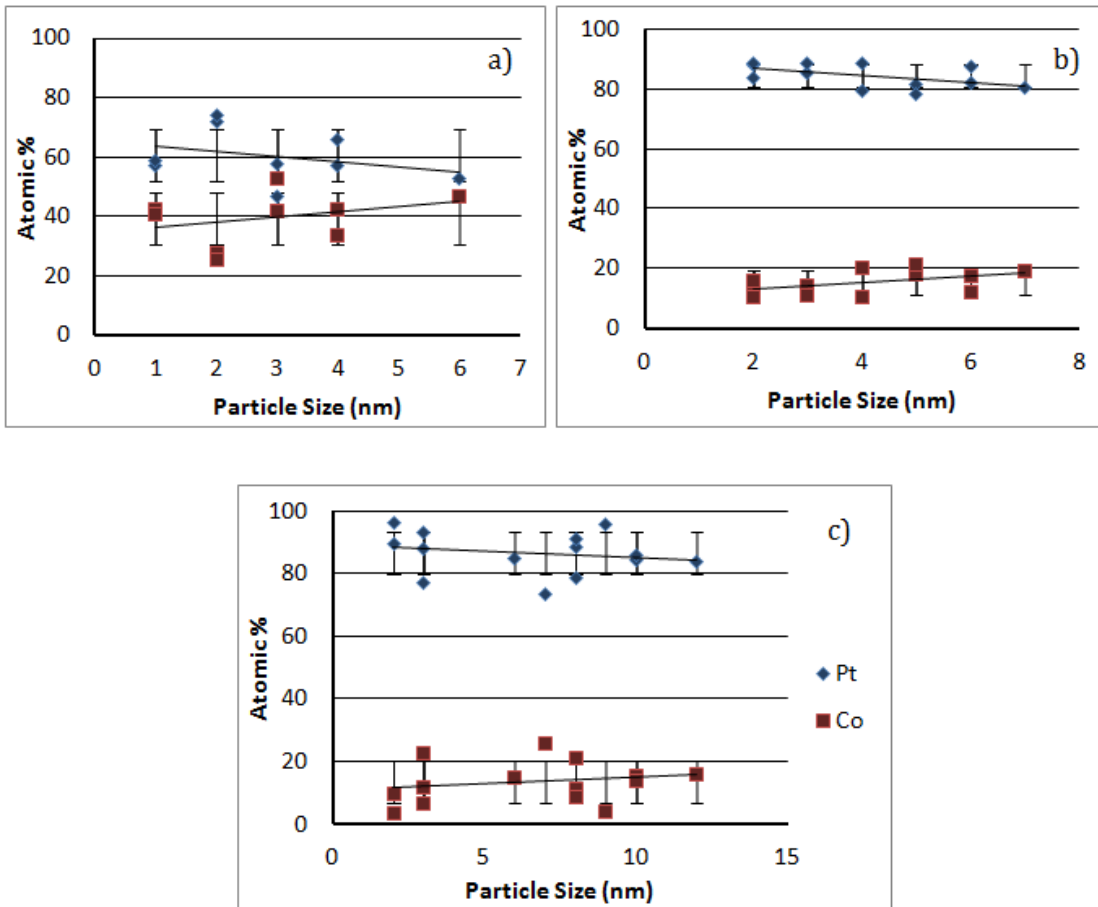
FIGURE 5-21 EDX SCAN OF PT-CO CORRELATING ATOMIC COMPOSITION WITH PARTICLE SIZE. A. B. AND C SHOWS RESULT FOR AS PREPARED, 60 CYCLES, AND 3000 CYCLES RESPECTIVELY

Figure 5-22 below correlates the atomic concentration with the cycling numbers. Unlike Figure 5-21, the EDXS data shown here are performed on catalyst clusters instead of individual nanoparticles. EDX data acquired in a larger area would produce more accurate results as more data acquisition points could be obtained. As expected, there are lower cobalt concentrations for the more cycled samples. In general, the EDXS results show that electrochemical cycling causes significant changes in atomic composition even with an electrochemical treatment as low as 60 cycles.
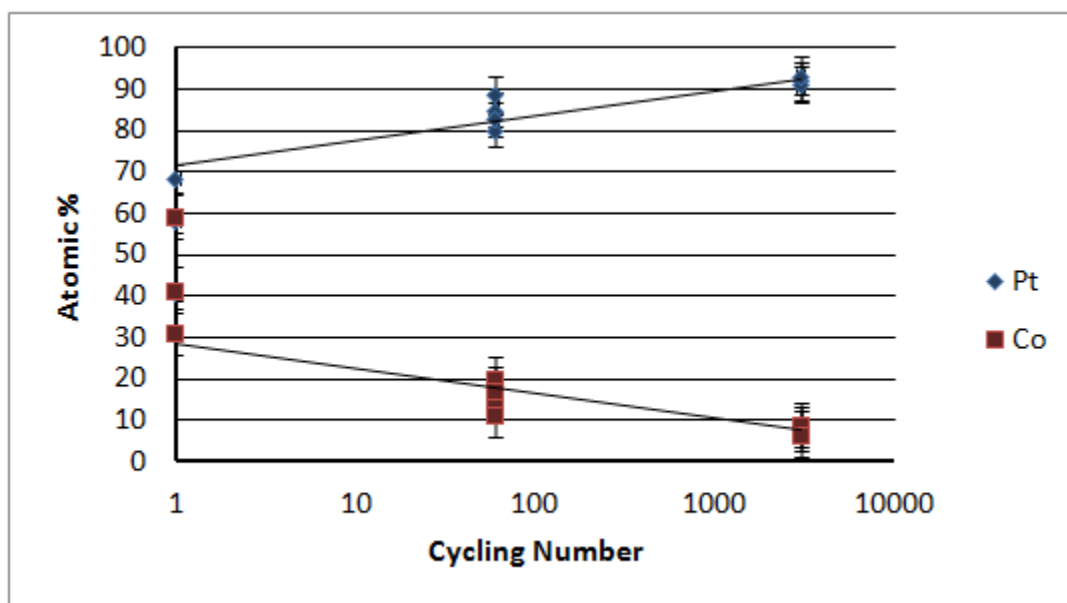
FIGURE 5-22 EDX SCAN OF CATALYST CLUSTERS CORRELATING ATOMIC COMPOSITION WITH CYCLING NUMBER

5.2.3. SURFACES AND MORPHOLOGY OF PT-CO NANOPARTICLES

Aberration corrected HAADF STEM imaging was performed in order to obtain detailed information on the surfaces and morphology of the Pt-Co nanocrystals. Figure

74

5-23 below shows a 5nm as synthesized Pt-Co nanoparticle viewing down the (110) zone axis. As depicted in Figure 5-23, there is a twin boundary with a slight mis-orientation that separates the two (110) orientations. Twin boundaries are known to be the nucleation sites where ordering initiates.[46] Aside from the twin plane, a number of facets can be identified around this particle including {011} and {001}. It is known that the edges at which these facets meet are excellent oxygen adsorption sites, along with all the mono atomic steps as indicated by the arrows. All these different defects and features make Pt-Co an excellent candidate for catalytic applications.
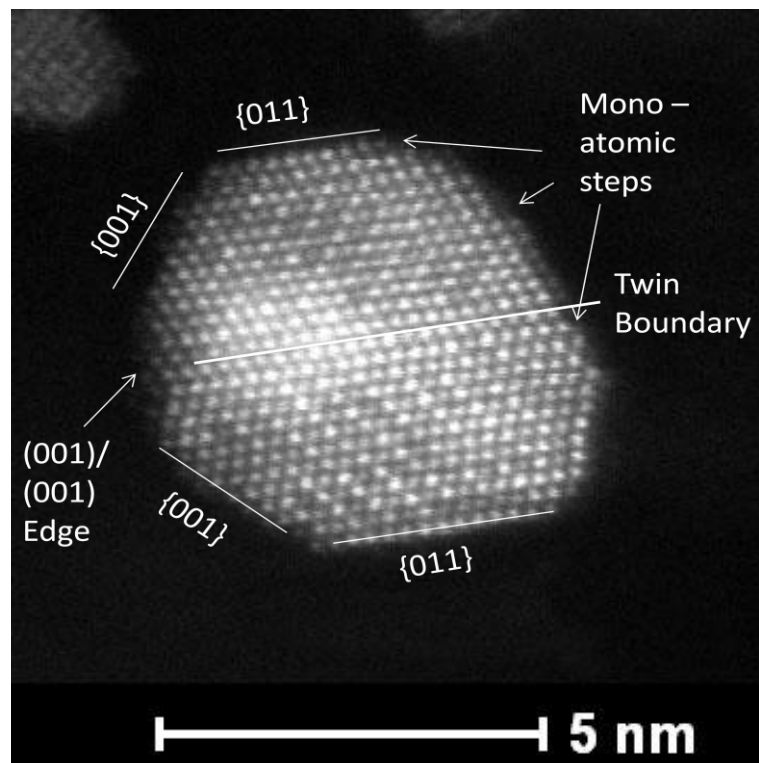
FIGURE 5-23 HAADF IMAGE OF 5NM PT-CO PARTICLE AT ZONE AXIS

Recall from the particle size distribution that the as-synthesized particles are very small with an average diameter of 2.7nm. Hence it was very difficult to locate isolated particles to identify the crystal orientation features. The series of images in Figure 5-24 show a number of nanoparticles orientated close to the zone axis. Although it is common for these catalysts to overlap, some useful insights can still be obtained from these images. Firstly, it can be observed that there is a low degree of ordering especially when compared with the Pt-Fe particles in Section 5.1. As indicated by the circled particles in Figure 5-24, there is an unclear atomic arrangement of these particles as no repeatable patterns can be observed. The ordering can be traced back to the synthesis process. These particles had a post annealing process at 600°C which, as reported by Alloyeau et. al., is the temperature that is beyond the critical temperature for particles less than 3nm in size. [33] In such case, a lower temperature annealing process would be more suitable for these Pt-Co particles to achieve higher ordering. Secondly, due to the nature of the small particles, it is unlikely that flat surface terrace would form. As indicated by the arrows in Figure 5-24 , there is a large number of surface defects including mono-atomic steps, kinks, ledges, twin planes, and edges. All of the listed defects could be adsorbent bonding locations that could maximize the number of active sites. However, it should be noted that these are as synthesized particles, thus the particle size would grow after electrochemical cycling and would decrease the number of these defects.
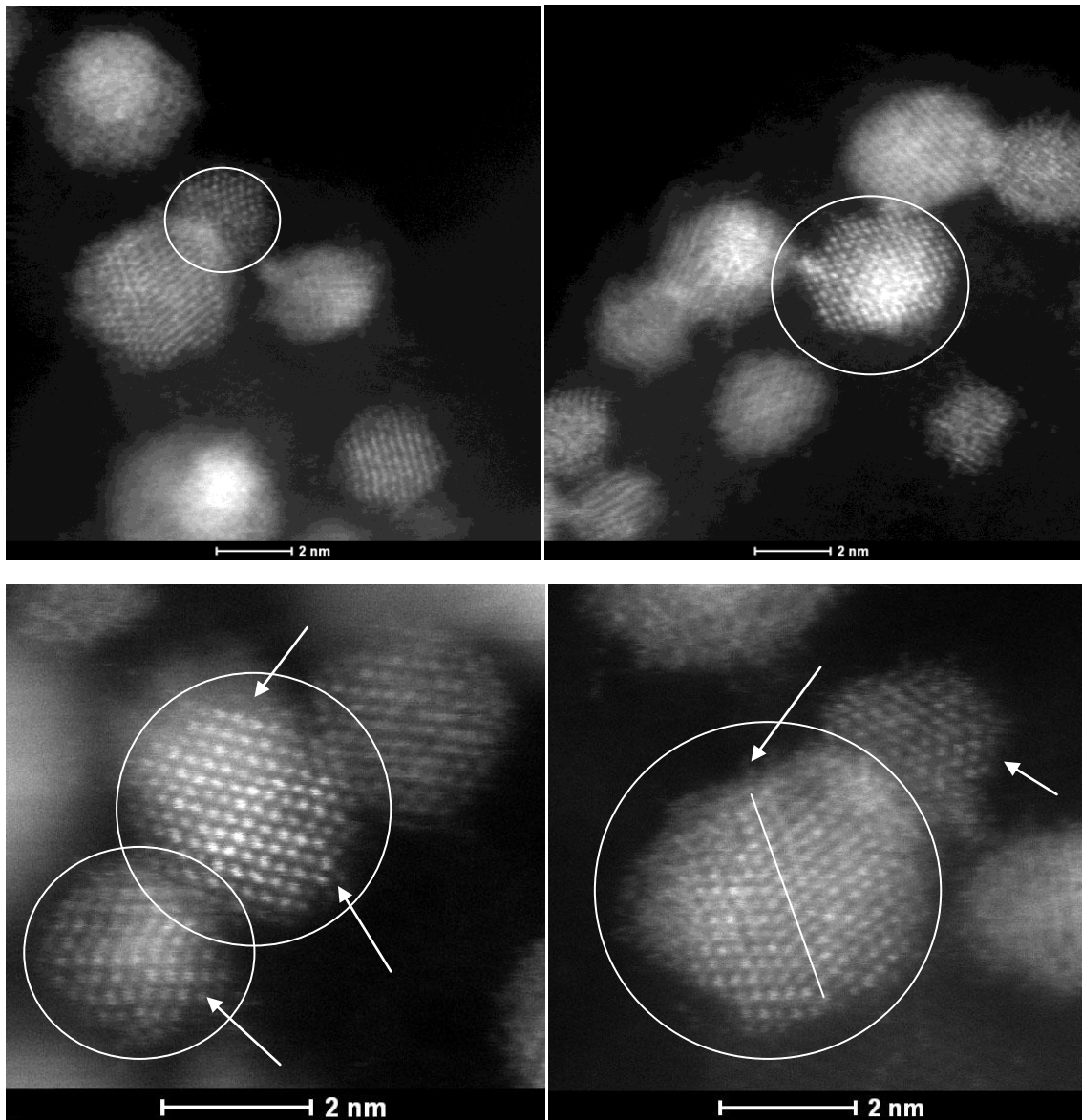
FIGURE 5-24 HAADF IMAGE OF VARIOUS AS PREPARED PT-CO NANOPARTICLES

Figure 5-25 below displays some atomically resolved images of Pt-Co nanoparticles that were cycled 3000 times. It is interesting to note that ordering can be observed as indicated by the circled areas. However, with a low sampling size of particles at its zone axis, it is difficult to determine and compare the degree of ordering of the as synthesized and cycled samples.

77
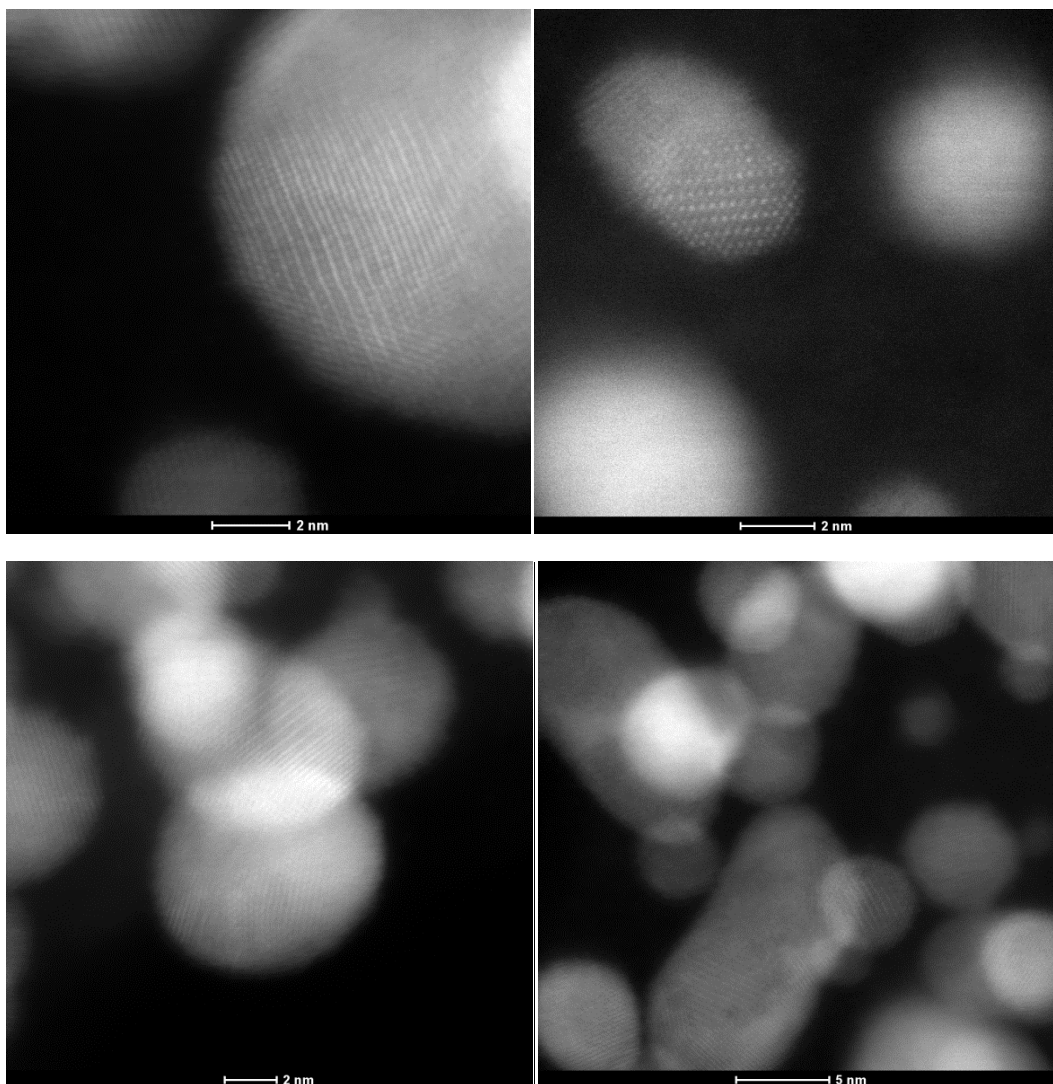
FIGURE 5-25 HAADF IMAGES OF VARIOUS ELECTROCHEMICALLY CYCLED PT-CO NANOPARTICLES

5.2.4. SUMMARY OF PT-CO CATALYTIC NANOPARTICLES

Pt-Co nanoparticles that were electrochemically treated at different cycling times (as synthesized, 60, and 3000 times) were characterized with transmission electron microscopy. The as synthesized particles appear to be small (size range 1 to

5 nm) and are densely populated on the Ketjen black high surface area carbon support. Cycling the samples 60 times caused no significant changes to the particle morphology but it caused major changes in the composition with lowered cobalt concentration after cycling. Cycling the samples 3000 times modifies both the morphology and composition of the catalysts. The particle sizes were remarkably larger with a broader (nearly doubled) size distribution as well as a drop in overall cobalt concentration to approximately 10%. High angle annular dark-field imaging shows low degree of ordering, as well as a number of low indexed planes and defects were identified. With the above information, higher atomic ordering could be achieved by adjusting the annealing temperature in the synthesis process. Lastly, the high number of surface defects would be beneficial for fuel cell catalysts as they act as active sites for the dissociation of hydrogen and oxygen.

6. CONCLUSIONS AND FURTHER WORK

The current research direction to seek a clean and environmentally friendly energy technology and fuel cells shows promising results with improved efficiency. However, a number of challenges must be resolved in order for this alternative energy system to be utilized globally. One of the major obstacles is to develop an alternatively stable and high activity catalyst in replacement of pure platinum. The use of platinum alloys show potential to be used as catalysts with enhanced activity and reduced platinum loading.

Two different platinum alloys including Pt-Fe and Pt-Co were studied down to the atomic level using aberration corrected transmission microcopy. Useful information such as the particle sizes, shapes, facets, degree of ordering, defects, and compositions were obtained which would aid in the process of catalyst development. The Pt-Fe particles were revealed to be highly ordered but with a relatively broad size distribution. On the other hand, Pt-Co shows a much better size control but with a low degree of ordering. With such information, chemists should then be able to modify the nanoparticle synthesis process to develop catalyst with enhanced performances.

The technique of energy dispersive X-rays microanalysis was utilized to extract composition information. Consistent in both of the alloys, it is shown that electrochemical cycling leads to a reduction in transition metal, increase in particle size,

80

as well as the detachment of the catalyst from the supporting material. In addition, it is revealed that electrochemical cycling could cause phase separation in which unique core shell structures could be form.

In terms of further work, the current emphasis of fuel cell research is placed on the catalyst and more in-depth understanding of factors including atomic ordering, and morphology could be performed. As part of atomic ordering of nanoparticles, there is currently no published literature with an experimental plot of ordering parameter vs. annealing temperature. Therefore, further research regarding quantitative measurement of degree of ordering on nanoparticles would be done to prove the theory. In addition, generally a bulk phase diagram cannot be used to describe the as synthesized nanoparticles since they are typically in a disordered state. Hence phase diagrams for nanoparticles are another possible future work.

Furthermore, the TEM work presented in this thesis only shows 2-dimensional evidence of active sites. It would be more accurate and representable if we understand the 3-dimensional structures of these nanoparticles. Thus techniques such as TEM tomography could be applied to obtain a 3-dimensional illustration of the catalyst. This would allow a precise measurement of location and frequency of the surface defects (kinks, steps, edges) that we identified with our TEM micrographs. Moreover, with the atomically resolved images that we acquired, discrete tomography could be utilized to

obtain a general 3-dimension figure of the particle based on the intensity of each atomic column.

Lastly, all the atomically resolved images presented in this thesis still contain useful information on the catalyst. Further image analysis could be done to extract information including atomic strain and compression. These information could then be related to the electrochemical performance to fine tune the catalytic ability of the nanoparticles.

Extensive research could be done with TEM to fully understand active sites on the surface of catalysts. A number of different microscopy techniques namely HAADF and EDXS could help to precisely understand the structure and surfaces of the nanoparticles. All in all, TEM is an unavoidable tool in the study and characterization of the nano- structures that would greatly contribute to the development of catalysts for fuel cell applications.

REFERENCES

[1]   M. Subhramannia and V. K. Pillai, "Shape-dependent electrocatalytic activity of platinum nanostructures," *Journal of Materials Chemistry*, vol. 18, pp. 5858-5870, 2008.

[2]   Y. Bing, H. Liu, L. Zhang, D. Ghosh, and J. Zhang, "Nanostructured Pt-alloy electrocatalysts for PEM fuel cell oxygen reduction reaction.," *Chemical Society reviews*, vol. 39, no. 6, pp. 2184-202, Jun. 2010.

[3]   B. S. Mun, M. Watanabe, M. Rossi, V. Stamenkovic, N. M. Markovic, and P. N. Ross, "A study of electronic structures of Pt3M (M=Ti,V,Cr,Fe,Co,Ni) polycrystalline alloys with valence-band photoemission spectroscopy.," *The Journal of chemical physics*, vol. 123, no. 20, p. 204717, Nov. 2005.

[4]   S. Mukerjee, S. Srinivasan, M. P. Soriaga, and J. Mcbreen, "Role of Structural and Electronic Properties of Pt and Pt Alloys on Electrocatalysis of Oxygen Reduction," *Journal of Electrochemical Society*, vol. 142, no. 5, pp. 1409- 1422, 1995.

[5]   Y. Lee, J. Rhee, and C. Whang, "Electronic structure of Co-Pt alloys: X-ray spectroscopy and density-functional calculations," *Physical Review B*, vol. 68, no. 23, pp. 1-7, Dec. 2003.

[6]   J. K. Nørskov et al., "Origin of the Overpotential for Oxygen Reduction at a Fuel-Cell Cathode," *Journal of Physical Chemistry B*, vol. 108, pp. 17886-17892, 2004.

[7]   Y. Xu, A. V. Ruban, and M. Mavrikakis, "Adsorption and dissociation of O2 on Pt-Co and Pt-Fe alloys.," *Journal of the American Chemical Society*, vol. 126, no. 14, pp. 4717-25, Apr. 2004.

[8]   V. Stamenkovic et al., "Changing the activity of electrocatalysts for oxygen reduction by tuning the surface electronic structure.," *Angewandte Chemie (International ed. in English)*, vol. 45, no. 18, pp. 2897-901, Apr. 2006.

[9]   T. J. Schmidt, V. Stamenkovic, P. N. Ross, and N. M. Markovic, "Oxygen Reduction Reaction on Pt and Pt Bimetallic Surfaces : A Selective Review," no. 2, pp. 105-116, 2001.

[10]   V. R. Stamenkovic et al., "Trends in electrocatalysis on extended and nanoscale Pt-bimetallic alloy surfaces.," *Nature materials*, vol. 6, no. 3, pp. 241-7, Mar. 2007.

[11]   T. Toda, H. Igarashi, and M. Watanabe, "Enhancement of the electrocatalytic O2 reduction on Pt – Fe alloys," *Journal of Electroanalytical Chemistry*, vol. 460, pp. 258-262, 1999.

[12]   P. Strasser et al., "Lattice-strain control of the activity in dealloyed core-shell fuel cell catalysts.," *Nature chemistry*, vol. 2, no. 6, pp. 454-60, Jun. 2010.

[13]   L. Y. Chang, A. S. Barnard, L. C. Gontard, and R. E. Dunin-Borkowski, "Resolving the structure of active sites on platinum catalytic nanoparticles.," *Nano letters*, vol. 10, no. 8, pp. 3073-6, Aug. 2010.

[14]   Y. Ding, Y. Gao, Z. L. Wang, N. Tian, Z.-Y. Zhou, and S.-G. Sun, "Facets and surface relaxation of tetrahexahedral platinum nanocrystals," *Applied Physics Letters*, vol. 91, no. 12, p. 121901, 2007.

[15]   Z. Gu and P. B. Balbuena, "Atomic Oxygen Absorption into Pt-Based Alloy Subsurfaces," *Journal of Physical Chemistry C*, vol. 112, no. 13, pp. 5057-5065, Apr. 2008.

[16]   M. Sanati, L. Wang, and A. Zunger, "Adaptive Crystal Structures: CuAu and NiPt," *Physical Review Letters*, vol. 90, no. 4, pp. 1-4, Jan. 2003.

[17]   Z. Peng and H. Yang, "Designer platinum nanoparticles: Control of shape, composition in alloy, nanostructure and electrocatalytic property," *Nano Today*, vol. 4, no. 2, pp. 143-164, Apr. 2009.

[18]   J. Ren and R. D. Tilley, "Shape-controlled growth of platinum nanoparticles.," *Small (Weinheim an der Bergstrasse, Germany)*, vol. 3, no. 9, pp. 1508-12, Sep. 2007.

[19]   S. S. Kim, C. Kim, and H. Lee, "Shape- and Composition-Controlled Pt–Fe–Co Nanoparticles for Electrocatalytic Methanol Oxidation," *Topics in Catalysis*, vol. 53, no. 7–10, pp. 686-693, Apr. 2010.

[20]   J. N. Kuhn, C.-K. Tsung, W. Huang, and G. a. Somorjai, "Effect of organic capping layers over monodisperse platinum nanoparticles upon activity for ethylene hydrogenation and carbon monoxide oxidation," *Journal of Catalysis*, vol. 265, no. 2, pp. 209-215, Jul. 2009.

[21]   W. Li, Q. Xin, and Y. Yan, "Nanostructured Pt–Fe/C cathode catalysts for direct methanol fuel cell: The effect of catalyst composition," *International Journal of Hydrogen Energy*, vol. 35, no. 6, pp. 2530-2538, Mar. 2010.

[22]   S. Zhang, X.-Z. Yuan, J. N. C. Hin, H. Wang, K. A. Friedrich, and M. Schulze, "A review of platinum-based catalyst layer degradation in proton exchange membrane fuel cells," *Journal of Power Sources*, vol. 194, no. 2, pp. 588-600, Dec. 2009.

[23]   Z. Peng, H. You, and H. Yang, "An Electrochemical Approach to PtAg Alloy Nanostructures Rich in Pt at the Surface," *Advanced Functional Materials*, pp. 3734-3741, 2010.

[24]   S. Chen, H. A. Gasteiger, K. Hayakawa, T. Tada, and Y. Shao-Horn, "Platinum-Alloy Cathode Catalyst Degradation in Proton Exchange Membrane Fuel Cells: Nanometer-

Scale Compositional and Morphological Changes," *Journal of The Electrochemical Society*, vol. 157, no. 1, p. A82, 2010.

[25]   C. Wang et al., "Multimetallic Au/FePt3 nanoparticles as highly durable electrocatalyst.," *Nano letters*, vol. 11, no. 3, pp. 919-26, Mar. 2011.

[26]   C. Wang, S. Peng, R. Chan, and S. Sun, "Synthesis of AuAg Alloy Nanoparticles from Core / Shell- Structured Ag / Au **," *Small Journal*, pp. 567-570, 2009.

[27]   K. Sasaki et al., "Core-protected platinum monolayer shell high-stability electrocatalysts for fuel-cell cathodes.," *Angewandte Chemie (International ed. in English)*, vol. 49, no. 46, pp. 8602-7, Nov. 2010.

[28]   K. J. J. Mayrhofer et al., "Fuel cell catalyst degradation on the nanoscale," *Journal of Physical Chemistry B*, vol. 10, pp. 1144-1147, 2008.

[29]   K. J. J. Mayrhofer, M. Hanzlik, and M. Arenz, "The influence of electrochemical annealing in CO saturated solution on the catalytic activity of Pt nanoparticles," *Electrochimica Acta*, vol. 54, no. 22, pp. 5018-5022, Sep. 2009.

[30]   K. J. J. Mayrhofer, S. J. Ashton, J. C. Meier, G. K. H. Wiberg, M. Hanzlik, and M. Arenz, "Non-destructive transmission electron microscopy study of catalyst degradation under electrochemical treatment," *Journal of Power Sources*, vol. 185, no. 2, pp. 734-739, Dec. 2008.

[31]   Y. Endo, N. Kikuchi, O. Kitakami, and Y. Shimada, "Lowering of ordering temperature for fct Fe–Pt in Fe/Pt multilayers," *Journal of Applied Physics*, vol. 89, no. 11, p. 7065, 2001.

[32]   D. Alloyeau, C. Langlois, C. Ricolleau, Y. Le Bouar, and a Loiseau, "A TEM in situ experiment as a guideline for the synthesis of as-grown ordered CoPt nanoparticles," *Nanotechnology*, vol. 18, no. 37, p. 375301, Sep. 2007.

[33]   D. Alloyeau et al., "Size and shape effects on the order-disorder phase transition in CoPt nanoparticles.," *Nature materials*, vol. 8, no. 12, pp. 940-6, Dec. 2009.

[34]   D. Alloyeau, C. Ricolleau, T. Oikawa, C. Langlois, Y. Le Bouar, and a Loiseau, "Comparing electron tomography and HRTEM slicing methods as tools to measure the thickness of nanoparticles.," *Ultramicroscopy*, vol. 109, no. 7, pp. 788-96, Jun. 2009.

[35]   B. Rellinghaus, S. Stappert, M. Acet, E. F. Wassermann, and a. Kowalik, "On the L10 Ordering Kinetics In Fe-Pt Nanoparticles," *INTERMAG 2006 - IEEE International Magnetics Conference*, vol. 42, no. 10, pp. 22-22, May 2006.

[36]   C. V. Rao and B. Viswanathan, "ORR Activity and Direct Ethanol Fuel Cell Performance of Carbon-Supported Pt-M (M) Fe , Co , and Cr) Alloys Prepared by Polyol Reduction Method," *Journal of Physical Chemistry C*, pp. 18907-18913, 2009.

[37]   Y. Li, L. Tang, and J. Li, "Preparation and electrochemical performance for methanol oxidation of pt/graphene nanocomposites," *Electrochemistry Communications*, vol. 11, no. 4, pp. 846-849, Apr. 2009.

[38]   M. Watanabe, "Activity and Stability of Ordered and Disordered Co-Pt Alloys for Phosphoric Acid Fuel Cells," *Journal of The Electrochemical Society*, vol. 141, no. 10, p. 2659, 1994.

[39]   A. K. Datye, Q. Xu, K. C. Kharas, and J. M. McCarty, "Particle size distributions in heterogeneous catalysts: What do they tell us about the sintering mechanism?," *Catalysis Today*, vol. 111, no. 1–2, pp. 59-67, Jan. 2006.

[40]   J. X. Wang et al., "Oxygen reduction on well-defined core-shell nanocatalysts: particle size, facet, and Pt shell thickness effects.," *Journal of the American Chemical Society*, vol. 131, no. 47, pp. 17298-302, Dec. 2009.

[41]   S. Peng, Y. Lee, C. Wang, H. Yin, S. Dai, and S. Sun, "A facile synthesis of monodisperse Au nanoparticles and their catalysis of CO oxidation," *Nano Research*, vol. 1, no. 3, pp. 229-234, Sep. 2008.

[42]   M. E. Gruner, "Chemical trends in structure and magnetism of bimetallic nanoparticles from atomistic calculations," *Journal of Physics D: Applied Physics*, vol. 43, no. 47, p. 474008, Dec. 2010.

[43]   N. Tian, Z.-Y. Zhou, S.-G. Sun, Y. Ding, and Z. L. Wang, "Synthesis of tetrahexahedral platinum nanocrystals with high-index facets and high electro-oxidation activity.," *Science (New York, N.Y.)*, vol. 316, no. 5825, pp. 732-5, May 2007.

[44]   Z. Dai, "Shapes, multiple twins and surface structures of monodisperse FePt magnetic nanocrystals," *Surface Science*, vol. 505, no. 1–2, pp. 325-335, May 2002.

[45]   C. Angeles-Chavez, P. Salas, T. Lopez-Luke, and E. de la Rosa, "High angle annular dark field-scanning transmission electron microscopy and high-resolution transmission electron microscopy studies in the Er2O3–ZrO2 system," *Vacuum*, vol. 84, no. 10, pp. 1226-1231, May 2010.

[46]   Z. R. Dai, S. Sun, and Z. L. Wang, "Phase Transformation , Coalescence , and Twinning of Monodisperse FePt Nanocrystals," *Nano Letters*, vol. 1, no. 001, 2001.

[47]   J. Ren and R. D. Tilley, "Shape Controlled Growth of Platinum Nanoparticles," *Small Journal*, no. 9, pp. 1508 - 1512, 2007.

[48]   S. Chen, Z. L. Wang, J. Ballato, S. H. Foulger, and D. L. Carroll, "Monopod, bipod, tripod, and tetrapod gold nanocrystals.," *Journal of the American Chemical Society*, vol. 125, no. 52, pp. 16186-7, Dec. 2003.

[49]   R. Callejastovar and P. Balbuena, "Oxygen adsorption and surface segregation in (211) surfaces of Pt(shell)/M(core) and Pt3M (M=Co, Ir) alloys," *Surface Science*, vol. 602, no. 22, pp. 3531-3539, Nov. 2008.

[50]   Z. L. Wang, "Transmission Electron Microscopy of Shape-Controlled Nanocrystals and Their Assemblies," *Journal of Physical Chemistry B*, pp. 1153-1175, 2000.

[51]   C. Liang, C. Bock, B. MacDougall, and P. H. J. Mercier, "Characteristics of Cubic and Tetragonal PtxFey/C and PtxFexCu/C Catalysts for the O2 Electro-Reduction," *ECS Transactions*, vol. 35, no. 34, pp. 69-80, 2011.

[52]   K. Du, F. Ernst, M. C. Pelsozy, J. Barthel, and K. Tillmann, "Expansion of interatomic distances in platinum catalyst nanoparticles," *Acta Materialia*, vol. 58, no. 3, pp. 836-845, Feb. 2010.

[53]   O. Gutfleisch, J. Lyubina, K.-H. Muller, and L. Schultz, "FePt Hard Magnets," *Advanced Engineering Materials*, vol. 7, no. 4, pp. 208-212, Apr. 2005.

[54]   S. J. L. Billinge and I. Levin, "The problem with determining atomic structure at the nanoscale.," *Science (New York, N.Y.)*, vol. 316, no. 5824, pp. 561-5, Apr. 2007.

[55]   S. Chen, H. a. Gasteiger, K. Hayakawa, T. Tada, and Y. Shao-Horn, "Platinum-Alloy Cathode Catalyst Degradation in Proton Exchange Membrane Fuel Cells: Nanometer-Scale Compositional and Morphological Changes," *Journal of The Electrochemical Society*, vol. 157, no. 1, p. A82, 2010.

[56]   "Fuel Cells Technical Plan," 2011.